PLOS Genetics

yippee like 3 (ypel3) is a novel gene required for myelinating and perineurial glia development

--Manuscript Draft--

Manuscript Number:	PGENETICS-D-19-01561
Full Title:	yippee like 3 (ypel3) is a novel gene required for myelinating and perineurial glia development
Short Title:	YPEL3 is a determinant of glial cell development
Article Type:	Research Article
Section/Category:	Natural Variation
Keywords:	human disease; genetic variant; glial cells; model organism
Corresponding Author:	Monte Westerfield University of Oregon Eugene, OR UNITED STATES
Corresponding Author's Institution:	University of Oregon
First Author:	Bernardo Blanco-Sanchéz
Order of Authors:	Bernardo Blanco-Sanchéz
	Aurélie Clément
	Sarah J Stednitz
	Jennifer Kyle
	Judy L Peirce
	Marcie McFadden
	Jeremy Wegner
	Jennifer B Phillips
	Ellen Macnamara
	Yan Huang
	David R Adams
	Camilo Toro
	William A Gahl
	May Christine V Malicdan
	Cynthia J Tifft
	Erika M Zink
	Kent J Bloodsworth
	Kelly G Stratton
	David Koeller
	Thomas O Metz
	Philip Washbourne
	Monte Westerfield
Abstract:	Hypomyelination, a neurological disorder characterized by a decrease in the production of myelin sheets by glial cells, often has no known etiology. Elucidating the genetic causes of hypomyelination provides a better understanding of myelination, as well as means to diagnose, council, and treat patients. Here, we present evidence that

Powered by Editorial Manager® and ProduXion Manager® from Aries Systems Corporation

	YIPPEE LIKE 3 (YPEL3), a gene whose developmental role was previously unknown, is required for central and peripheral glial cell development. We identified a child with a constellation of clinical features including cerebral hypomyelination, abnormal peripheral nerve conduction, hypotonia, areflexia, and hypertrophic peripheral nerves. Exome and genome sequencing revealed a de novo mutation that creates a frame-shift in the open reading frame of YPEL3 , leading to an early stop codon. We used zebrafish as a model system to validate that YPEL3 mutations are causative of neuropathy. We found that ypel3 isexpressed in the zebrafish central and peripheral nervous system. Using CRISPR/Cas9 technology, we created zebrafish mutants carrying a genomic lesion similar to that of the patient. Our analysis revealed that Ypel3 is required for specification and migration of myelinating oligodendrocytes, timely exit of the perineurial glial precursors from the central nervous system (CNS), formation of the perineurium, and Schwann cell maturation. Consistent with these observations, zebrafish ypel3 mutants have metabolomic signatures characteristic of oligodendrocyte and Schwann cell differentiation defects, show decreased levels of Myelin basic protein in the central and peripheral nervous system, and develop defasciculated peripheral nerves. Locomotion defects were observed in adult zebrafish ypel3 mutants. These studies demonstrate that Ypel3 is a novel gene required for perineurial cell differentiation and glial myelination.
Suggested Reviewers:	Sarah Kucenas University of Virginia sk4ub@virginia.edu
	Kelly Monk Oregon Health Science University monk@ohsu.edu
	Bruce Appel University of Colorado Denver bruce.appel@ucdenver.edu
	Liliana Solnica-Krezel Washington University in Saint Louis School of Medicine solnical@wustl.edu
Opposed Reviewers:	
Additional Information:	
Question	**Response**
Financial Disclosure Enter a financial disclosure statement that describes the sources of funding for the work included in this submission. Review the submission guidelines for detailed requirements. View published research articles from *PLOS Genetics* for specific examples. This statement is required for submission and **will appear in the published article** if the submission is accepted. Please make sure it is accurate.	M.W., GM114438, NS093793, National Institutes of Health, nih.gov, NO. K.D.M. and T.O.M., TR001395, National Institute of Health, nih.gov. NO. T.O.M., DEAC05-76RLO1830, United States Department of Energy, energy.gov. NO.

Powered by Editorial Manager® and ProduXion Manager® from Aries Systems Corporation

Unfunded studies Enter: *The author(s) received no specific funding for this work.* **Funded studies** Enter a statement with the following details: • Initials of the authors who received each award • Grant numbers awarded to each author • The full name of each funder • URL of each funder website • Did the sponsors or funders play any role in the study design, data collection and analysis, decision to publish, or preparation of the manuscript? • **NO** - Include this sentence at the end of your statement: *The funders had no role in study design, data collection and analysis, decision to publish, or preparation of the manuscript.* • **YES** - Specify the role(s) played. * typeset	
Competing Interests Use the instructions below to enter a competing interest statement for this submission. On behalf of all authors, disclose any competing interests that could be perceived to bias this work—acknowledging all financial support and any other relevant financial or non-financial competing interests. This statement **will appear in the published article** if the submission is accepted. Please make sure it is accurate. View published research articles from *PLOS Genetics* for specific examples.	NO

Powered by Editorial Manager® and ProduXion Manager® from Aries Systems Corporation

NO authors have competing interests Enter: *The authors have declared that no competing interests exist.* **Authors with competing interests** Enter competing interest details beginning with this statement: *I have read the journal's policy and the authors of this manuscript have the following competing interests: [insert competing interests here]* * typeset	
Data Availability Authors are required to make all data underlying the findings described fully available, without restriction, and from the time of publication. PLOS allows rare exceptions to address legal and ethical concerns. See the PLOS Data Policy and FAQ for detailed information. A Data Availability Statement describing where the data can be found is required at submission. Your answers to this question constitute the Data Availability Statement and will be published in the article, if accepted. **Important:** Stating 'data available on request from the author' is not sufficient. If your data are only available upon request, select 'No' for the first question and explain your exceptional situation in the text box. Do the authors confirm that all data underlying the findings described in their manuscript are fully available without restriction?	Yes - all data are fully available without restriction

Powered by Editorial Manager® and ProduXion Manager® from Aries Systems Corporation

Describe where the data may be found in full sentences. If you are copying our sample text, replace any instances of XXX with the appropriate details. • If the data are **held or will be held in a public repository**, include URLs, accession numbers or DOIs. If this information will only be available after acceptance, indicate this by ticking the box below. For example: *All XXX files are available from the XXX database (accession number(s) XXX, XXX.*). • If the data are all contained **within the manuscript and/or Supporting Information files**, enter the following: *All relevant data are within the manuscript and its Supporting Information files.* • If neither of these applies but you are able to provide **details of access elsewhere**, with or without limitations, please do so. For example: *Data cannot be shared publicly because of [XXX]. Data are available from the XXX Institutional Data Access / Ethics Committee (contact via XXX) for researchers who meet the criteria for access to confidential data.* *The data underlying the results presented in the study are available from (include the name of the third party and contact information or URL).* • This text is appropriate if the data are owned by a third party and authors do not have permission to share the data. * typeset	All data are contained within the manuscript and/or Supporting Information files
Additional data availability information:	

Powered by Editorial Manager® and ProduXion Manager® from Aries Systems Corporation

UNIVERSITY OF OREGON

September 17, 2019

To the Editor,

We submit our manuscript, "*yippee like 3* (*ypel3*) is a novel gene required for myelinating and perineurial glia development", to consider for publication in *PLoS Genetics*.

Our study shows that *YPEL3* function is required for myelinating oligodendrocyte precursors, Schwann cell maturation, and perineurial glial cell development. The role of *YPEL3* during embryogenesis was previously unknown.

This work on *YPEL3* was inspired by a patient that entered our program and who is affected by an undiagnosed clinical condition characterized by central nervous system (CNS) hypomyelination and defasciculated peripheral nerves. The patient´s whole exome sequence revealed a variant of unknown significance characterized by a frameshift that introduces 38 abnormal amino acids and premature stop codon into the *YPEL3* gene.

We created a zebrafish model carrying a similar mutation. Our studies reveal that, in zebrafish, loss of Ypel3 function causes hypomyelination in the CNS, and perturbs Schwann cell maturation and perineurial glial development, leading to defasciculated peripheral nerves. Thus, zebrafish *ypel3* mutants recapitulate the CNS hypomyelination and peripheral nerve defects presented by the patient. This study identifies YPEL3 as a new determinant of glial cell development.

Sincerely

Monte Westerfield, Ph.D.
Professor of Biology
Member, Institute of Neuroscience
Director, ZFIN and the Zebrafish International
Resource Center

MONTE WESTERFIELD

INSTITUTE OF NEUROSCIENCE

1254 University of Oregon, Eugene OR 97403-1254 **T** (541) 346-4607 **F** (541) 346-4548 **E** monte@uoregon.edu

An equal-opportunity, affirmative-action institution committed to cultural diversity and compliance with the Americans with Disabilities Act

Manuscript Click here to download Manuscript Blanco.pdf

TITLE:

***yippee like 3* (*ypel3*) is a novel gene required for myelinating and perineurial glia development**

SHORT TITLE:

YPEL3 is a determinant of glial cell development

AUTHORS:

Bernardo Blanco-Sánchez[1,#], Aurélie Clément[1], Sara J. Stednitz[1], Jennifer Kyle[2], Judy L. Peirce[1], Marcie McFadden[1], Jeremy Wegner[1], Jennifer B. Phillips[1], Ellen Macnamara[3,4], Yan Huang[3], David R. Adams[3,4], Camilo Toro[3,4], William A. Gahl[3,5], May Christine V. Malicdan[3,4], Cynthia J. Tifft[3,4], Erika M. Zink[2], Kent J. Bloodsworth[2], Kelly G. Stratton[2], David Koeller[6], Thomas O. Metz[2], Philip Washbourne[1], Monte Westerfield[1]

Affiliations

[1] Institute of Neuroscience, University of Oregon, Eugene, OR 97403, USA

[2] Pacific Northwest National Laboratory, Richland, WA 99354, USA

[3] National Institutes of Health Undiagnosed Diseases Program, Common Fund, Office of the Director, National Institutes of Health, Bethesda, MD 20892, USA

[4]Office of the Clinical Director, National Human Genome Research Institute, National Institutes of Health, Bethesda, MD 20892, USA

[5]Section of Human Biochemical Genetics, Medical Genetics Branch, National Human Genome Research Institute, National Institutes of Health, Bethesda, MD 20892, USA

[6]Molecular and Medical Genetics, School of Medicine, Oregon Health and Science University, Portland, OR 97239, USA

Current address: Institut Imagine, UMR1163, Paris 75015, FRANCE

Contact information

* Corresponding authors: bernardo.blanco@institutimagine.org; monte@uoregon.edu

ABSTRACT

Hypomyelination, a neurological disorder characterized by a decrease in the production of myelin sheets by glial cells, often has no known etiology. Elucidating the genetic causes of hypomyelination provides a better understanding of myelination, as well as means to diagnose, council, and treat patients. Here, we present evidence that *YIPPEE LIKE 3 (YPEL3),* a gene whose developmental role was previously unknown, is required for central and peripheral glial cell development. We identified a child with a constellation of clinical features including cerebral hypomyelination, abnormal peripheral nerve conduction, hypotonia, areflexia, and hypertrophic peripheral nerves. Exome and genome sequencing revealed *a de novo* mutation that creates a frame-shift in the open reading frame of *YPEL3*, leading to an early stop codon. We used zebrafish as a model system to validate that *YPEL3* mutations are causative of neuropathy. We found that *ypel3* is expressed in the zebrafish central and peripheral nervous system. Using CRISPR/Cas9 technology, we created zebrafish mutants carrying a genomic lesion similar to that of the patient. Our analysis revealed that Ypel3 is required for specification and migration of myelinating oligodendrocytes, timely exit of the perineurial glial precursors from the central nervous system (CNS), formation of the perineurium, and Schwann cell maturation. Consistent with these observations, zebrafish *ypel3* mutants have metabolomic signatures characteristic of oligodendrocyte and Schwann cell differentiation defects, show decreased levels of Myelin basic protein in the central and peripheral nervous system, and develop defasciculated peripheral nerves. Locomotion defects were observed in adult zebrafish *ypel3* mutants. These studies demonstrate that Ypel3 is a novel gene required for perineurial cell differentiation and glial myelination.

AUTHOR SUMMARY

The study of congenital rare diseases allows the identification of new gene variants involved in development. Genetic and sequence analysis of a patient with a novel complex phenotype

including hypomyelination, enlarged peripheral nerves, and motor defects implicated a *de novo* mutation in the *YPEL3* gene as potentially causative. *YPEL3* had not previously been associated with disease. Using CRISPR technology, we created a zebrafish model carrying a DNA lesion similar to that of the affected patient. Homozygous mutant embryos display weak and variable peripheral nerve phenotypes and are viable. Because *ypel3* transcripts are present from fertilization, we generated maternal zygotic mutants. Analysis of these mutants revealed hypomyelination, defective axonal wrapping, and swimming defects. Time-lapse video lineage analysis showed that *ypel3* is required for oligodendrocyte specification, Schwann cell differentiation, and proper perineurial cell development. These results identify YPEL3 as a new determinant of glial cell development and support the conclusion that the *de novo YPEL3* mutation is responsible for the patient's disease.

INTRODUCTION

Myelin is a vertebrate-specific, specialized lipid-rich sheath that functions to increase nerve conduction [1-3]. Myelin is essential for neural circuitry function and thus for sensory, motor, and cognitive functions [4]. Within the developing spinal cord, myelinating oligodendrocytes originate from the ventral neural tube [5-9]. Progenitor cells (pMNs) first produce motoneuron progenitors and then switch to generate oligodendrocyte progenitor cells (OPCs) [6,10-12]; those that coexpress Sox10 and Nkx2.2 transcription factors are fated to become myelinating OPCs [8,13-15]. Myelinating oligodendrocytes migrate along and myelinate developing axons in the central nervous system (CNS) and myelinate them [16,17]. Defects in any of these processes can result in CNS hypomyelination. In the peripheral nervous system (PNS), Schwann cells produce myelin [18,19]. Unlike OPCs, Schwann cells are neural crest derivatives. During their migration and interaction with peripheral axons, they express Sox10 [20-22]. Combinatory expression of Sox10, YAP, and NFATc4 marks the promyelinating stage [21,23,24]. These transcription factors induce expression of Krox20, an essential transcriptional activator that drives peripheral

79 myelination [18]. Therefore, loss of function of common factors involved in the differentiation or
80 promyelination programs of both OPCs and Schwann cells, such as Sox10, should impair
81 myelination in both the CNS and PNS.
82
83 Perineurial glia are also required for peripheral nerve development [25,26]. They form the
84 perineurium, an epithelial cell layer that ensheaths Schwann cells and peripheral axons, and
85 whose function is similar to that of the blood-brain barrier [27-29]. Perineurial glia associated
86 with motor axons originate from the second most ventral domain of the developing spinal cord,
87 called the p3 domain [26,29,30]. Motor axon associated perineurial cells leave the CNS at
88 determined exit points, where they migrate in a chain-like fashion along the developing motor
89 nerve [26,29]. During motor nerve morphogenesis, Schwann cells are necessary for proper
90 differentiation of perineurial glia [25,26] and reciprocally, perineurial glia are required for proper
91 myelination by Schwann cells, as well as peripheral nerve fasciculation [26,30]. Disruption of
92 instructive interactions between perineural glia and Schwann cells results in peripheral nerve
93 dysmorphogenesis.
94
95 We identified of a *de novo* heterozygous mutation in the *YPEL3* gene of a patient with CNS
96 hypomyelination and hypertrophic peripheral nerves; this suggested that YPEL3 may function in
97 glia cell development. *YPEL3* was first identified as a pro-senescence factor in a screen for
98 genes induced during the apoptotic phase of myeloid cell development [31]. *YPEL3* belongs to
99 the evolutionarily conserved *Yippee-Like* gene family [32]. Its subcellular localization is highly
100 dynamic during the cell cycle. YPEL3 localizes within the nucleus in a salt and pepper pattern,
101 but is found in an unidentified perinuclear structure during interphase, and near the
102 centrosomes during mitosis [32]. Genetic studies have shown that, under genotoxic stress,
103 *YPEL3* is an inducible target of P53 [33]. In breast, lung, colon, ovarian, and nasopharyngeal
104 carcinoma cells, *YPEL3* expression is downregulated [33-35]. Overexpression of *YPEL3* in

105 cultured cells results in cell cycle arrest [31,33] and suppression of the epithelial-mesenchymal
106 transition in nasopharyngeal carcinoma cells [35]. These data from cell culture models and
107 tumor samples suggest that YPEL3 functions as a tumor suppressor. However, the role of
108 YPEL3 in development remains unknown.
109
110 To validate the genetic basis of the patient's disease and to study YPEL3 function during
111 embryonic development, we created a Ypel3 loss-of-function zebrafish that mimics the patient's
112 mutation. Our results show that zebrafish depleted of Ypel3 have locomotor defects and that
113 Ypel3 is required for specification and migration of myelinating oligodendrocyte, timely exit of
114 the perineurial glia from the developing spinal cord, formation of the perineurium, Schwann cell
115 maturation, and CNS and PNS myelination. Thus, we propose that Ypel3 is a novel gene
116 required for myelinating and perineurial glia development.
117
118 **RESULTS**
119 **A de novo *YPEL3* variant is a rare disease-causing candidate allele**
120 The patient (UDP_2179) is a Caucasian female who was evaluated at the NIH Undiagnosed
121 Diseases Program (NIHUDP) at 6 years of age. She was born to a nonconsanguineous union,
122 and has two older siblings who are relatively healthy. However, her mother had two
123 miscarriages. The patient presented with gross and fine motor developmental delay, proximal
124 and distal weakness, lymphedema, profound hypotonia, joint laxity, sleep apnea, and failure to
125 thrive. She had feeding difficulties, with severe gastroesophageal reflux disease (GERD) that
126 required a G-tube placement at 8 months of age. On examination, the patient had normal
127 weight (22.3 kg, 50-75th %ile), height, (120 cm, 25-50th %ile), and body mass index (15.4 kg/m2,
128 50-75th %ile). She required maximal assistance to come from a supine to a sitting position but
129 could maintain good sitting balance and roll independently from side-to-side. Cranial nerves
130 were normal. Muscle strength was 2-3/5 in the upper extremities, with no clear strength in the

hand intrinsics, and 0-1 in the lower extremities. She had mild flexion contractures at the interphalangeal joints of both hands, hip, knees, and ankles. Protective sensation to 5.07 monofilament was intact, but subjectively decreased in a glove distribution.

Nerve conduction studies and electromyogram were consistent with a neurogenic process with motor and sensory abnormalities, with significant demyelinating features and axonal loss. Muscle biopsy at 5 years of age showed no primary muscle pathology. MRI of upper and lower extremities showed massive dilation of peripheral nerves throughout the brachial plexus (**Fig 1A**), and in the sciatic, tibial and femoral nerves in the legs, with complete sparing of the cranial nerves and no extension into the spinal cord. The cross sectional diameters of these nerves in the arm range from 1 to 1.5 cm, with each individual nerve appearing to be composed of a number of engorged fascicles. The caliber of the nerve in the brachial plexus was greater than the diameter of the humerus. There was atrophy throughout the muscles in the arms but erector muscles in the back appeared to be spared. In the lower extremities, there was marked symmetric diffuse muscle atrophy and fatty infiltration with relative sparing of the adductors. Brain MRI revealed diffuse cerebral hypomyelination comparable to that of a 10 to 12-month-old (Fig 1B).

Exome sequencing revealed a variant of unknown significance, NM_031477.4(*YPEL3*):c.273dup. This duplication leads to a frameshift, p.Val92Serfs*38, in both long and short YPEL3 transcript variants. Clinical genome sequencing did not reveal additional variants.

155 ***ypel3* is evolutionarily conserved and expressed in the CNS and developing motor**
156 **nerves**
157 To investigate the genetic basis of the patient's disease and YPEL3 function during embryonic
158 development, we used zebrafish. *ypel3*, the zebrafish gene orthologous to human *YPEL3*,
159 encodes a protein that is 89% identical and 94% similar to the human protein (**Sup. Fig 1A**). We
160 found that *ypel3* is maternally deposited (**Fig 1C**) and strongly expressed from 24-80 hours
161 postfertilization (hpf) in the developing CNS within the ventricular and mantle zones, but is
162 excluded from the marginal zone (**Figs 1D-E**). CNS development is characterized by a biphasic
163 mode of differentiation [6,36,37]. During the first phase, progenitor domains give rise to distinct
164 arrays of neuronal precursors, including motoneurons. The second phase starts when these
165 progenitor domains switch to generate different types of glial precursor cells [38]. In zebrafish,
166 the pMN produces motoneurons until approximately 26-30 hpf [10]. Then and throughout the
167 second phase, the pMN domain cells gives rise to the myelinating oligodendrocyte lineage,
168 whereas p3 precursor cells generate CNS glia and perineurial cells [26,30]. At 24 and 56 hpf,
169 we observed *ypel3* expression in the progenitor domains of the developing spinal cord, including
170 the pMN and p3 domains, and in cells in the region of the developing motor roots (red arrows in
171 **Fig 1D-E**) where both perineurial and Schwann cell precursors are found [25,26,30]. At 80 hpf,
172 *ypel3* expression was maintained within the progenitor domains of the CNS, as well as in the
173 region of the developing motor roots (**Fig 1F**).
174
175 ***ypel3*^{b1309} and *ypel3*^{b1310} CRISPR engineered alleles are equivalent to *de novo YPEL3***
176 **variant**
177 Differentiation defects in motoneurons, myelinating oligodendrocytes, Schwann cells and/or
178 perineurial glia could potentially explain the morphological and physiological phenotypes
179 observed in the patient carrying the *de novo* mutation in the *YPEL3* gene. Thus, we engineered
180 *ypel3* CRISPR alleles to study the gene's role in development.

181

182 We generated *ypel3*^{b1309} and *ypel3*^{b1310} zebrafish mutant alleles using the CRISPR/Cas9 system
183 and a guide RNA targeting the junction between intron 3 and exon 4 (see Materials and
184 Methods). The *b1309* allele (p.N56Gfs*1) has a 4 base pair (bp) substitution and a 1 bp
185 insertion, whereas the *b1310* allele (p.G60Rfs*4) carries a 7 bp insertion (**Sup. Fig 1B**). As a
186 consequence, the open reading frame is shifted and an early stop codon is introduced by each
187 mutation, resulting in a frameshift similar to that of the patient (p.V54Sfs*38, based on the short
188 *YPEL3* isoform NP_1138996.1) (**FIG 1 G**,**H, Sup. Fig 1B**).

189

190 **Maternal zygotic *ypel3* mutants have behavioral and locomotor defects**

191 We then characterized motoneuron and glial differentiation in homozygous F2 generations (see
192 material and methods). Analysis of both *ypel3*^{b1309} and *ypel3*^{b1310} homozygous mutants revealed
193 rather subtle and variable phenotypes. Considering that maternally deposited *ypel3* products
194 (Fig. 1C) might provide sufficient function for early development, we generated maternal-zygotic
195 (mz) mutants to remove the maternal contribution. We raised homozygous *ypel3* mutants to
196 adulthood and crossed homozygous mutant females to their heterozygous mutant males to
197 generate mz *ypel3* mutants for both alleles. During the first 5 days of embryonic development,
198 there were no gross morphological or behavioral phenotypes in either of mz *ypel3* mutant
199 genotype, and mz *ypel3* mutants were viable.

200

201 We raised mz *ypel3* mutants to adulthood and analyzed their swimming behavior (total distance
202 the fish traveled, preference for tank space occupancy, and time in motion) [39] compared to
203 that of wild-type (WT) and heterozygous siblings **(Fig 2A-F)**. The total distance traveled did not
204 differ among any genotypes ($p > 0.950$ in all cases) **(Fig 2D)**. In contrast, mz *ypel3* mutants and
205 heterozygous fish exhibited a significant preference for the bottom of the tank as measured by
206 average relative distance from the surface of the water compared to WT siblings ($p < 0.001$ in

207 both cases), and were similar to each other (p = 0.832) **(Fig 2E)**. Strikingly, mz *ypel3* mutants
208 spent less time in motion than both heterozygous and WT siblings (p = 0.020 and 0.011,
209 respectively), whereas heterozygotes and WT behavior did not differ (p = 0.946) **(Fig 2F)**. This
210 effect is explained by a greater frequency of pauses by the mz *ypel3* mutants during their
211 swimming trajectories compared to siblings (p = 0.032 and p = 0.013).
212
213 To identify the cellular cause of the swimming defect, we analyzed development of neural
214 circuitry, with a particular emphasis on motoneuron, myelinating oligodendrocyte, and peripheral
215 glia differentiation.
216
217 **Specification of the pMN and motoneuron differentiation are normal in the *mz ypel3***
218 **mutants**
219 To analyze pMN specification, we used the *Tg*[*olig2:kaede*] transgenic line, which labels the
220 pMN domain and its derivatives [10,40]. We crossed the transgene into the *ypel3* heterozygous
221 mutant male background. Then, we crossed the transgenic *ypel3* heterozygous males to *ypel3*
222 heterozygous or homozygous mutant females. WT (n=10) and transgenic mz *ypel3*$^{b1310/b1310}$
223 mutant (n=10) embryos were collected at 24 hpf, fixed, individually genotyped, sectioned
224 transversely, and analyzed at the level of somites 6 to 12 (**FIG 3A-F**). Sections were co-stained
225 with an anti-Kaede antibody and the nuclear maker Topro3 to facilitate cell counting within the
226 pMN domain (**Fig 3A,B,D,E**). In zebrafish at 24 hpf, the pMN is composed of 2-3 cells organized
227 in a column adjacent to the luminal region of the developing spinal cord (**Fig 3C,F)** [10]. We did
228 not observe any changes in the extension of the pMN along the luminal region of the spinal
229 cord, nor in the number of Kaede-positive cells in the CNS per section.
230
231 Motoneuron differentiation was assayed by counting cells that express the *Tg*[*mnx1:GFP*]
232 transgene, a live marker of differentiated motoneurons [41] that we crossed into the *ypel3*^{b1310}

233 heterozygous background. We then crossed these males with *ypel3* heterozygous or
234 homozygous mutant females and used a spinning disk microscope to image 26 hpf embryos
235 and 52 hpf larvae, laterally, at the level of somites 7-10 **(Fig 3F-J)**. Each imaged embryo or
236 larva was then individually genotyped. Quantification of the GFP-positive cells revealed no
237 statistically significant difference between WT and mz *ypel3* mutants at any of the stages
238 studied (n=10 for each genotype per stage of interest). Thus, *ypel3* is not required for pMN
239 specification or for motoneuron differentiation.
240
241 ***ypel3* is required for specification of myelinating oligodendrocytes**
242 OPCs coexpressing *nkx2.2a* and *sox10* differentiate into myelinating oligodendrocytes [8,42].
243 Myelinating oligodendrocytes can then be identified by their expression of the *myelin basic*
244 *protein* (*mbp*) gene [43,44]. Thus, we studied myelinating oligodendrocyte specification using
245 dual live colabeling of oligodendrocyte precursors cells (OPCs) using the *Tg*[*sox10:mRFP*] and
246 *Tg*[*nkx2.2a: GFP*] transgenes [8,17], referred as *sox10:mRFP* and *nkx.2.a:GFP*, respectively,
247 here after. As expected, the *nkx2.2a:GFP* transgene was also detected in the ventral p3 domain
248 of the spinal cord [8]. In our experiments, *ypel3*^{b1310} heterozygous males carried the
249 *nkx2.2a:GFP* transgene, whereas the *sox10:mRFP* construct was carried by either *ypel3*^{b1310}
250 heterozygous or homozygous mutant females.
251
252 After crossing the transgenic *ypel3* heterozygous males with their respective transgenic *ypel3*
253 heterozygous or homozygous females, we fixed double mRFP- and GFP-positive larvae at 56
254 hpf, and genotyped each larva. WT (n=9) and mz *ypel3* (n=10) mutant larvae were labeled with
255 antibodies recognizing GFP and mRFP. The average number of double GFP and mRFP
256 positive cell bodies localized dorsal to the p3 domain were quantified per somite between
257 somites 6 and 12 (**Fig 4A, C**). We found a statistically significant 50% decrease in the number
258 of myelinating OPCs in the mz *ypel3* mutants compared to WT. At this stage, in WT larvae, the

259 average number of myelinating OPCs was 3 per somite, whereas in the mz *ypel3* mutant this
260 number varied between 1 and 2 (**Fig 4E**).
261
262 To understand the consequences of these reduced numbers of OPCs, we performed live
263 imaging using a spinning disc microscope. For this, we mounted double mRFP- and GFP-
264 positive larvae laterally and recorded OPC development from 50 hpf to 62 hpf at the level of
265 somites 8-10, followed by genotyping. Analysis of the time-lapse videos revealed that, from 50
266 hpf, the number of myelinating OPCs was constant in WT larvae, suggesting that no new cell
267 bodies within the region of interest (localized dorsal of the p3 domain) were added (**Sup. video**
268 **1**). However, in the mz *ypel3* mutants, myelinating OPCs were absent at 50 hpf (t=0) (**Sup.**
269 **video 2**), and from 54 hpf, only a few presumptive myelinating mz *ypel3* mutant OPCs, derived
270 from the ventral p3 domain, were observed migrating dorsally. These mz *ypel3* OPCs did not
271 transition to the pyramidal shape typical of differentiating OPCs, but rather maintained a more
272 rounded, mesenchymal-like morphology (arrows in **Sup. video 2**). Additionally, mz *ypel3* mutant
273 OPCs failed to extend filopodia, which are necessary for correct axonal wrapping and
274 myelination (**Sup. video 2**) [17,44,45].
275
276 During the migratory process, these mz *ypel3* OPCs stayed closer to each other, forming
277 clumps rather than scattering along the anteroposterior CNS axis, a repulsion phenomenon
278 necessary for correct axonal wrapping and myelination within the CNS (**Sup. video 2**) [17,46].
279 As a consequence, segments of the spinal cord were depleted of OPCs. We assayed
280 myelination by OPCs at 72 hpf by *in situ* hybridization (ISH) of *mbpb* expression (**Fig 4B,D**), and
281 observed a 50% decrease in the number of *mbpb*-positive cells in mz *ypel3* mutants when
282 compare to WT (**Fig 4F**). We counted the number of *mbpb*-positive cells in the spinal cord
283 region localized between somites 6 to 10. In WT. The *mbpb*-positive cells were located at the
284 anterior and posterior ends of each somite, producing a uniform pattern **(Fig 4B, arrows**); each

285 somite segment contained an average of two *mbpb*-positive cells **(Fig 4F**). In the mz *ypel3*
286 mutants, each somite segment had an average of one *mbpb*-positive cell **(Fig4 F).** Mutant
287 *mbpb*-positive cells were discontinuously distributed such that somites were often devoid of
288 *mbpb*-positive cells whereas others contained clusters randomly distributed within the somite
289 **(Fig 4D)**. We also observed these phenotypes by time-lapse recording of OPC development
290 and migration in the *mz ypel3* mutant (arrows in sup. **Sup. video 2**).
291
292 To determine whether the decrease in myelinating OPC number was due to cell death or a
293 defect in cell proliferation, we performed TUNEL (terminal deoxynucleotidyl transferase dUTP
294 nick end) and EDU (5-ethynyl-2'-deoxyuridine) labeling, respectively. TUNEL staining was
295 performed in 32, 56 and 72 hpf WT and *mz ypel3* mutants. Larvae were analyzed at the level of
296 the spinal cord between somites 6 to 12. At all stages, the number of TUNEL-positive cells was
297 zero for both WT and mutants (n=45 for each stage and genotype). We observed TUNEL signal
298 in the heart at these stages, as a positive control. These experiments ruled out cell death as a
299 cause for the decrease in the number of myelinating OPCs.
300
301 We then performed EDU pulse and chase experiments to study cell division. The "pulse" group
302 was fixed at 52 hpf and the "chase" group was fixed at 72 hpf. There was no statistically
303 significant difference in the average number of EDU-positive cells per larva at 52 and 72 hpf
304 between WT and *mz ypel3* mutants **(Fig 4G,H).** These cell proliferation experiments showed
305 that *ypel3* loss of function does not affect the cell cycle during CNS development. Together,
306 these results strongly suggest that Ypel3 function is specifically required for myelinating
307 oligodendrocyte specification rather than OPC proliferation or survival.
308
309

310 **Ypel3 is required for proper maturation of Schwann cell precursors**

311 Enlarged peripheral nerves are one of the most striking phenotypes of the patient (**Fig. 1A**).
312 Taking advantage of the *Tg*(*olig2:kaede)* and *Tg*(*mnx1:GFP*) transgenic lines that label
313 motoneuron cell bodies and their corresponding axons, we found no differences in the width of
314 axon bundles at 24 and 52 hpf between mz *ypel3* mutants and WT siblings (**sup Fig2**)**.** This
315 suggested that the hypertrophic nerve defect does not have a neuronal origin.

316

317 Expression of *ypel3* mRNA was detected in cells localized within the motor roots (**Fig. 1E**).
318 Therefore, we examined development of peripheral glia to determine whether *ypel3* is required
319 for peripheral motor nerve morphogenesis. Schwann and perineurial cells are the two types of
320 glial cells required for peripheral motor axon insulation and fasciculation (Kucenas, 2015). We
321 labeled Schwann cells with the *sox10:mRF*P transgene and perineurial cells with the
322 *nkx2.2:GFP* transgene. Time lapse recording of mz *ypel3* mutants from 50 to 60 hpf revealed
323 that perineurial glia (green arrows in **Sup. video 1**) did not exit the CNS in a timely manner and
324 failed to wrap the developing motor nerves (**compare Sup. videos 1,2**).

325

326 Motor axon ensheathing can be characterized as a 3-step process. First, Schwann cell
327 precursors (SCP) migrate ventrally and encounter the developing axons. During this step, the
328 SCPs differentiate into immature Schwann cells and associate with motor axons, forming tube-
329 like structures. In zebrafish, the second step starts around 40-48 hpf [26], when perineurial glia
330 leave the CNS and migrate along the immature motor nerve. Perineurial glia envelop the
331 immature Schwann cells, becoming part of the tubular structure. During the third step of
332 “tightening” or “compaction”, both glial cell types become tightly associated with each other and
333 perineurial cells ensheath the axons and associated Schwann cells, forming the perineurium.
334 This tightening process can be visualized by studying the formation of slender rods that

335 emanate from the ventral roots toward the horizontal myotome, and the co-expression of
336 markers labeling both Schwann and perineurial cells.
337
338 In zebrafish, SCPs and immature Schwann cells are labeled by the *sox10:mRFP* transgene
339 and Schwann cell maturation correlates with the progressive fading of transgene expression in a
340 ventral to dorsal gradient along the motor nerve [26]. Thus, we characterized initial Schwann
341 cell development by assaying the expression of *sox10* at 26 hpf using colorimetric whole-mount
342 *ISH* and Nomarski microscopy. Surprisingly, *sox10* expression levels were elevated in the mz
343 *ypel3* mutant Schwann cells compared to WT (**Fig 5A,B**; n=15 for each experiment). When we
344 assayed Schwann cell localization at this stage labeled as mRFP-positive cells along the motor
345 nerve, we did not observe any differences (**Fig 5C,D**). This suggested that high levels of *sox10*
346 expression did not affect SCP migration.
347
348 At 56 hpf, during the early steps of the second phase of motor axon ensheathing, Schwann cell
349 localization and morphology along the motor nerve were undistinguishable between mz *ypel3*
350 mutant and WT (**Fig 5E,F)**. In addition, scoring mRFP-positive cells along the motor axon,
351 revealed that essentially all motor nerves are associated with Schwann cells (**Fig 5I**) in both WT
352 and *mz ypel3* mutants.
353
354 At 5 dpf, during the late stages of the third phase of motor axon ensheathing, WT Schwann cells
355 have acquired the typical slender rod morphology and *sox10:mRFP* expression has faded from
356 the ventral myotome region (**Fig 5G**, white arrows). In the mz *ypel3* mutants, however, 100% of
357 Schwann cells failed to acquire the slender rod morphology, and *sox10:mRFP* expression was
358 maintained in the ventral myotome (**Fig 5H**, red arrows, **J**). This suggested a defect in Schwann
359 cell maturation in the mz *ypel3* mutant.
360

361 **Ypel3 is required for perineurial glia development**

362 Perineurial glial cells derive from the p3 domain in the ventral region of the developing spinal
363 cord. This domain and its cell derivatives are labeled by the *nkx2.2:mGFP* transgene. In
364 zebrafish, perineurial cells start exiting the CNS by 40 hpf and migrate along the motor nerve to
365 continue their development and formation of the perineurium [26].

366 We used time-lapse videos from 50 to 60 hpf to track GFP-positive perineurial cells exiting the
367 spinal cord and found that perineurial glia failed to migrate properly along the immature motor
368 nerves in mz *ypel3* mutants. In WT, this migratory process is highly dynamic, as perineurial cells
369 actively extend and retract cellular processes along their migratory track, contacting and
370 wrapping Schwann cells, and finally forming a tubular structure (**Sup. video 1**). In mz *ypel3*
371 mutants, very few perineurial glia were observed. A few filopodia sometimes emanated from the
372 spinal cord, but no cell bodies (**Sup. video 2**). To quantify defects, we scored the presence of
373 GFP-positive perineurial cells associated with mRFP-positive Schwann cells along the motor
374 axons. WT and mz *ypel3* mutant larvae were fixed at 56 hpf, a relatively well-advanced stage for
375 the wrapping of the immature nerve by the perineurial cells, and antibody labeling for both
376 mGFP and mRFP was performed. 80% of the analyzed WT motor nerves were associated with
377 perineurial glia (**Fig 6A,E**), and perineurial glia formed highly distinguishable tubular structures
378 that enveloped the base of the motor axon and Schwann cells from the spinal cord to the
379 horizontal myoseptum (**Fig 6A,** white arrow and dashed white line, respectively). In *mz ypel3*
380 mutants, on the other hand, the percentage of motor nerves associated with perineurial glia was
381 40%, a reduction of 50% in comparison to WT (**Fig 6C,E**). In addition, the few mutant perineurial
382 cells that migrated out from the CNS failed to form rod-like structures, indicative of a defect in
383 wrapping (**Fig 6C**, yellow arrow).

384

385 To learn whether these defects were due simply to a delay in development, we grew the larvae
386 to 5 dpf and labeled them as described above. As expected, we observed slender rods

387 colabeled with mRFP and GFP in WT (**Fig 6C**, white arrow), showing that the tightening phase
388 is being executed properly. A few loose perineurial glia were observed around the slender rods
389 (**Fig 6B**, asterisks). However, in *mz ypel3* mutants, we observed overgrown perineurial glia, as
390 indicated by expression of the *nkx2.2:mGFP* transgene, that formed enlarged and swollen
391 tubular structures. These large nerves (**Fig 6D**) were very similar to the hypertrophic nerves
392 observed in the patient (**Fig 1A**). By 5 dpf in WT siblings, 90% of the peripheral glia associated
393 with motor nerves (n=22) had acquired a slender rod morphology (**Fig 6C,F**), but this
394 percentage was only 25% in the mz *ypel3* mutants (n=22) (**Fig 6D,F**). Structurally, WT slender
395 rods at 7 dpf were composed of a tubular perineurial cell layer that encapsulated the mature
396 Schwann cells (**Fig 6G**, arrow, **G''** and **G'**, respectively), which progressively extinguished
397 *sox10:mRFP* transgene expression. At the same stage, perineurial cells in mz *ypel3* mutants
398 were very disorganized and failed to form a slender tubule. Instead, they gave rise to a swollen
399 partitioned perineurium, and the motor nerve was defasciculated as visualized with mRPF
400 expression in Schwann cells (**Fig 6H-H''**). These results indicate that mutant perineurial glia do
401 not develop properly and fail to ensheath Schwann cells and motor axons, hence compromising
402 the structural integrity of the perineurium and contributing to nerve defasciculation.
403
404 **mz *ypel3 mutants* have elevated levels of phosphatidic acids and very long-chained**
405 **ceramides and lower levels of Myelin basic protein-B and galactolipids**
406 To characterize cellular phenotypes of the mutant Schwann and perineurial cells that could
407 potentially play a role in their failure to differentiate, we performed comparative lipidomics
408 analysis of WT and mz *ypel3* mutant zebrafish larvae at 7 dpf. For this, 5 independent replicates
409 of 400-500 larvae each were collected at 7 dpf, frozen in liquid nitrogen and processed for
410 lipidomics analysis. The mz *ypel3* mutants had altered levels of sphingomeylin, ceramides, and
411 phosphatidic acids and compared to WT (**Fig 7E)**. Sphingomyelins, major lipid components of
412 myelin membranes, are decreased in *ypel3* except for those containing a fatty acid chain of 24

413 carbons or greater. The ceramide species that are statistically elevated also contain longer
414 chain fatty acids (C25 and C26). Fatty acid chain length has been linked to neuronal cell death
415 [47,48]. Previous studies in the CNS have shown that galoctosphingolipids, ceramide
416 derivatives that are all decreased in this study (**Fig 7E**), act as regulators of oligodendrocyte
417 differentiation [49]. Phosphatidic acids were elevated in mz *ypel3* mutants, and previous studies
418 in the PNS showed that high levels of phosphatidic acids negatively regulate Schwann cell
419 differentiation and myelination through the activation of the MEK-ERK pathway [49]. Thus,
420 defects in OPC and Schwann cell terminal differentiation in mz *ypel3* mutants may be due to
421 changes in lipid composition.
422
423 We further examined myelinating oligodendrocyte and Schwann cell terminal differentiation in 7
424 dpf larvae by whole-mount immunolabeling of Myelin basic protein-b (Mbp-b), a marker of this
425 late developmental step. We detected Mbp-b expression within the CNS and along each motor
426 nerve fascicle in 100% of WT larvae (n=12) (**Fig 7A**). In mz *ypel3* mutants, Mbp-b was
427 undetectable in the CNS of 100% of larvae (n=14). Moreover, Mbp-b signal was discontinuous
428 in mz *ypel3* mutant motor nerves and weaker than in WT in 79% of the cases (10/14). Mbp-b
429 signal often highlighted defasciculated nerves in these mutants (**Fig 7B,C**, arrows). In the
430 remaining 21% (3/14), Mbp-b was undetectable in the motor nerves (**Fig 7D**).
431
432 **DISCUSSION**
433 The developmental role of Ypel3 was previously unknown. Our studies demonstrate that *ypel3*
434 is required for specification, migration, and terminal differentiation of myelinating
435 oligodendrocytes and Schwann cells. In addition, Ypel3 function is required for differentiation of
436 perineurial glia and morphogenesis of the peripheral nerve perineurium. Despite broad
437 expression of *ypel3* in the developing spinal cord, we find that neither pMN specification nor
438 motoneuron differentiation is affected in *ypel3* mutants. Similarly, there is no sign of increased

439 cell death or decreased cell proliferation. On the other hand, onset of the earliest known
440 markers for myelinating OPC lineage (*sox10* and *nkx2.2*) is delayed, and later differentiation of
441 OPCs is defective. Lipidomics and molecular analysis of terminal differentiation using Mbp-b as
442 a marker suggests that the few specified myelinating OPCs fail to differentiate properly. Thus,
443 our data suggest that Ypel3 function is required rather specifically for specification and
444 differentiation of perineurial and myelinating glial cells.
445
446 Temporal delay in the appearance of myelinating OPCs in the *mz ypel3* mutants, as observed
447 with time-lapse microscopy, suggests that Ypel3 influences the timely onset of the pro-
448 myelinating transcriptional cascade regulated by Sox10 and Nkx2.2 transcription factors. Delay
449 in the onset of this cascade results in a decrease in the total number of myelinating OPCs
450 formed, as in *Nkx2.2* mouse mutants [42]. In addition, the few presumptive mz *ypel3* mutant
451 myelinating OPCs that do form have abnormal mesenchyme-like morphologies and a tendency
452 to clump. These two defects, the decrease in the population of myelinating OPCs and their
453 incorrect migratory pattern, are likely contributors to the hypomyelination [17,44,46] we
454 observed in the *ypel3* mutants. Future studies to understand how Ypel3 promotes myelinating
455 OPC specification and differentiation, will need to identify Ypel3 interactors and the downstream
456 biochemical pathways affected in the mutant and whether Ypel3 influences OPC specification
457 as myelinating oligodendrocytes or NG2 glial lineages by modulating Shh and Notch activity
458 [50].
459
460 An important driving force during peripheral nerve morphogenesis is the establishment of
461 instructive interactions between perineurial glia and Schwann cells [25,26,30]. Disruption in
462 these interactions causes peripheral defasciculation and hampers myelination by Schwann
463 cells. During motor nerve development, both perineurial and Schwann cells are affected in *ypel3*
464 mutants. Although high levels of *sox10* expression are maintained, Schwann cells still migrate

465 toward the motor axons. Similarly, initial wrapping of the motor nerve by Schwann cells occurs
466 normally, around 56 hpf. However, by 5 and 7 dpf wrapping defects are evident when Schwann
467 cells fail to form slender rods, stop expressing the immature Schwann cell transgene marker
468 *sox10:mRFP*, and fail terminal differentiation as indicated by the Mbp-b expression. Further, our
469 lipidomics analysis revealed elevated levels of phosphatic acids in mz *ypel3* mutants compared
470 to WT, a dysregulation associated with impaired Schwann cell differentiation [51]. These rather
471 late stage defects in Schwann cell differentiation correlate with the time that perineurial glia form
472 the perineurium. On the other hand, our data indicate that *ypel3* is necessary much earlier for
473 the timely exit of perineurial glia from the CNS and their association with Schwann cells. We
474 propose that initial failure of perineurial glia migration disrupts the instructive interaction
475 between Schwann cells and perineurial glia. As a consequence, Schwann cells cannot
476 differentiate properly and Mbp-b levels are decreased in mz *ypel3* mutant motor nerves. In
477 support of this interpretation, in both mouse and zebrafish models depleted of perineurial cells,
478 Schwann cells fail to differentiate properly and nerves have severe myelination and fasciculation
479 defects, [26,30], as we observed in mz *ypel3* mutants.
480
481 YPEL3 has been proposed to act as a negative regulator of the WNT/ß-Catenin signaling
482 pathway by preventing ß -Catenin nuclear translocation during metastasis of nasopharyngeal
483 carcinoma cells [35]. According to this model, YPEL3 blocks the epithelial-mesenchymal
484 transition by stabilizing cytoplasmic ß-Catenin levels, although the regulatory mechanism has
485 not been elucidated, and no evidence of a physical interaction between YPEL3 and ß -Catenin
486 has been provided so far. Interestingly, the overgrowth of perineurial cells we observe in mz
487 *ypel3* mutants is reminiscent of a dysregulated or defective epithelial-mesenchymal transition.
488 Although WNTs are implicated in distinct aspects of neural development, their role in perineurial
489 glia morphogenesis is unclear. To understand Ypel3 function in motor nerve development,
490 dissection of the role of Ypel3 in the transition of perineurial cells from the neural epithelium to

491 their mesenchymal migratory state and the contribution of Schwann cells to this developmental
492 step will be necessary.
493
494 Our interest in *YPEL3* arose from a patient with a variant of unknown significance in this gene
495 who displays unique clinical features including central hypomyelination and peripheral
496 neuropathy. Our aim was to test whether mutations in *YPEL3* could be responsible for these
497 symptoms. Our data show that zebrafish *ypel3* mutants recapitulate the CNS hypomyelination
498 and peripheral nerve defects presented by the patient. Identification of additional patients with
499 *YPEL3* mutations and overlapping phenotypes will provide further confidence that *YPEL3* is a
500 neuropathy gene.
501
502 **MATERIALS AND METHODS**
503
504 **Patient enrollment/consent**
505 The patient was evaluated at the National Institutes of Health Undiagnosed Diseases Program
506 (NIH UDP) [52-54] and was enrolled in the protocol 76-HG-0238, approved by the National
507 Human Genome Research Institute Institutional Review Board. Her parents provided written
508 informed consent.
509
510 **Exome sequence/Genomic analysis**
511 Whole exome sequencing analysis was performed on the patient and her parents at the
512 National Institutes of Health Intramural Sequencing Center (NISC). Peripheral whole blood
513 samples were collected for DNA extraction using AutoGen FLEX STAR. Phenol-chloroform
514 purified DNA were prepared enriched for targeted whole exome regions using the TruSeq DNA
515 Sample Prep Kit v1 (Illumina, San Diego, CA) and sequenced on the HiSeq 2000 Sequencing
516 System (Illumina, San Diego, CA) for 101-bp paired-end reads. The sequencing reads then

517 were filtered for quality and aligned to human reference genome NCBI build 37 (hg19) using
518 pipeline developed by the Undiagnosed Diseases Program (UDP), one based on NovoAlign
519 (Novocraft Technologies, Petaling Jaya, Malaysia), and separately, a diploid aligner[55] that
520 was run on a commercial platform (Appistry Inc., St. Louis, MO). Variants were called with
521 HaplotypeCaller and GenotypeGVCFs.[56-58] Variants were annotated using snpEff[59] and a
522 combination of publicly available data sources (ExAC, ESP, 1000Genomes, see URLs) and
523 internal cohort statistics, manually inspected using the Integrative Genomics Viewer (IGV), and
524 checked for publicly available clinical or functional data in OMIM, HGMD, and PubMed. Variants
525 were interpreted and prioritized based on the clinical relevance of the gene and the
526 pathogenicity of the variants using the ACMG-AMP guidelines [60] or inferred significance
527 based on Mendelian consistency, population frequency, and predicted deleteriousness.
528 Clinical genome sequencing was performed by HudsonAlpha (Huntsville, AL).
529

530 **Fish strains**

531 Homozygous WT (*ypel3*$^{+/+}$), heterozygous mutants (*ypel3*$^{+/b1309}$ and *ypel3*$^{+/b1310}$), homozygous
532 mutants (*ypel3* $^{b1309/b1309}$ and *ypel3*$^{b1310/b1310}$), maternal-zygotic homozygous mutants (mz *ypel3*
533 $^{b1309/b1309}$ and mz *ypel3*$^{b1310/b1310}$), *Tg[olig2:kaede]*^{vu85} [40]; *Tg Bac[nkx2.2:mGFP]*^{vu16} [17],
534 *Tg[mnx1:GFP]*^{ml12} [41] and *Tg[sox10(7.2):mRFP]*^{vu234} [8], and WT strain ABCxTu adult zebrafish
535 were maintained as previously described [61]. Embryos and larvae were staged according to
536 the standard staging series [62], by hours postfertilization (hpf), or days postfertilization (dpf).
537 Adults stocks of *ypel3*$^{+/+}$, *ypel3*$^{+/b1309}$ and *ypel3*$^{+/b1310}$, *ypel3*$^{b1309/b1309}$ and *ypel3*$^{b1310/b1310}$ were
538 generated by incrossing F2, F3 and F4 heterozygous *ypel3* mutant adults. WT controls
539 (*ypel3*$^{+/+}$) used for comparative analysis with mz *ypel3* mutants were obtained by crossing adults
540 *ypel3*$^{+/+}$ females with heterozygous adults *ypel3*$^{+/b1309}$ or *ypel3*$^{+/b1310}$ males. mz *ypel3*$^{b1309/b1309}$ and
541 mz *ypel3*$^{b1310/b1310}$ were obtained by crossing homozygous *ypel3* $^{b1309/b1309}$ or homozygous
542 *ypel3*$^{b1310/b1310}$ females with *ypel3*$^{+/b1309}$ and *ypel3*$^{+/b1310}$ heterozygous males, respectively. All

543 experimental samples were genotyped. All experimental procedures were approved by the
544 University of Oregon IACUC.
545
546 **Protein identity and similarity analysis**
547 The DRSC Integrative Ortholog Prediction Tool (DIOPT) freeware (Hu Y et al., 2011) was used
548 to determine protein identity and similarity between human YPEL3 (NP_113665.3), the product
549 encoded by the long human *YPEL3* transcript, and zebrafish Ypel3 (NP_997955.1) proteins.
550 The *YPEL3* gene encodes two transcript variants, a long variant (NM_031477) giving rise to a
551 protein composed of 157 amino acids and a short variant (NM_001145524) giving rise to a
552 protein of 119 amino acid. Only one zebrafish *ypel3* transcript variant has been characterized to
553 date that encodes a protein of 119 amino acids.
554
555 **RT-PCR and cloning of *ypel3* coding sequence**
556 RNA was extracted from 26 hpf ABCxTu embryos. PCR was performed after retro-transcription
557 using the SuperScript® III First-Strand Synthesis System. Primers used were: *ypel3* forward: 5'-
558 CAAACATCCAGACATGGTGAAG-3', *ypel3* reverse: 5'-CGGTGACAGCAAGTTAAATACAAA-
559 3'.
560
561 ***In Situ* Hybridization (ISH)**
562 Embryos and larvae were hybridized with a digoxigenin labeled RNA probe spanning the entire
563 coding sequence of *ypel3*. For wholemount ISH, we used the previously published protocol [63].
564 ISH experiments on zebrafish 16 µm thick cryosections were performed using previously
565 described protocols [64], with the following modifications: hybridization and washes were
566 performed at 70 °C, and anti-digoxigenin antibody dilution was 1:5000. Images of samples
567 labeled by ISH were acquired using a Zeiss Axioplan2 compound microscope.
568

569 **Generation of indel mutant lines using CRISPR**

570 To create the *ypel3* mutant line using the CRISPR/Cas9 system, an RNA guide targeting the 5'-
571 GgtgtttttagGGTGAACGT-3' sequence at the level of intron3-exon4 junction was designed.
572 Indels were identified using the following primers: Forward 5'-GTAAATGGTTGGGACGTAGCG-
573 3'; Reverse 5'-TTTGGCATCGGTTCTGTTAAA-3'. Two different indels were recovered,
574 *ypel3*^{b1309} (p. p.N56Gfs*1) and *ypel3*^{b1310} (p.G60Rfs*4). Both F0 carriers were crossed with
575 ABCxTu to generate an F1 stable line. Identified F1 *ypel3* heterozygous mutant fish were
576 outcrossed with a different ABCxTu family to generate an F2 generation. Our phenotypic
577 characterization was performed from the F2 stocks and derived fish families.

578

579 **Behavioral assay**

580 Locomotor behavior was assessed in a novel tank test, where individual animals were placed
581 into a custom glass tank measuring 25 cm (width) x 24 cm (height) x 2.5 cm (depth) illuminated
582 with a white LED panel (Environmental Lights). Images were obtained at 10 Hz using a Logitech
583 webcam, and tracking was performed on the fly using a modified form of DaniOPEN [39]. The
584 percentage of time in motion was calculated by dividing the number of frames where the
585 animal's position moved one third of its body length by the total number of frames acquired.
586 Pauses were defined as a period of time where animals were immobile for a minimum of 1
587 second.

588

589 **Immunolabeling**

590 Labeling of wholemount larvae was performed following our published protocol [65] with minor
591 modifications. Embryos at 52 hpf and 5 dpf and 7dpf larvae were anesthetized with MS-222
592 (tricaine-S; Syndel USA) at 4 g/l, fixed in BT fix overnight. Embryos at 52 hpf were
593 permeabilized in 1.5% tween-20 in PBS for 18 hours. Larvae at 5 and 7 dpf were permeabilized
594 in 2.5% tween-20 in PBS for 18 hours or 48 hours, respectively. To perform immunolabeling of

595 sections, samples were genotyped and sorted accordingly to genotypes. WT and mz *ypel3*
596 mutant embryos were embedded in 1% agarose/0.5% agar/5% sucrose and 16 µm cryosections
597 were cut. For single and double immunolabeling, following a 2-hour blocking step (PBS + 0.01%
598 Tween-20 + 5% bovine serum albumin + 5% goat serum), the larvae were incubated overnight
599 at 4°C with primary antibodies. Primary antibodies were rabbit anti-GFP directly coupled with
600 Alexa488 (cat#A-21311, Life technologies, dilution 1:400), rabbit dsRed (cat#632496, Clontech,
601 dilution 1:200), rabbit anti-Kaede (cat#PM012, MBL International, dilution 1:250), rabbit anti-
602 Mbp-b (kind gift from Bruce Appel, dilution 1/100) (Hines et al., 2015). TOPRO (cat#T3605, Life
603 technologies) was reconstituted in PBS following manufacturer's recommendations. Sections
604 were incubated overnight at 4°C in a 1/1000 diluted TOPRO reconstituted solution. For double
605 labeling of GFP and mRFP, sequential detection was used, during which mRFP signal was
606 amplified first using anti-dsRED followed by the addition of a goat anti-rabbit Alexa 555
607 secondary antibody (cat# A-21428, Life technologies, dilution 1:500). After 6 washes of 30
608 minutes each and a 2 hour blocking step, samples were incubated with an anti-rabbit GFP
609 directly coupled to Alexa488. Sections and wholemount samples were imaged in vectashield
610 medium (cat#H-1000, Vectorlabs) using a Zeiss LSM 5 confocal microscope.
611
612 **TUNEL labeling**
613 TUNEL staining was performed as previously described with minor modifications [66]. Apoptag
614 plus Peroxidase *In situ* Apoptosis Detection Kit was used (manufacturer). Larvae at 32, 52, and
615 76 hpf were anesthetized with MS-222, fixed in BT fix overnight, and stored overnight in 100%
616 methanol. After rehydration, the larvae were permeabilized for 20, 30, and 40 minutes in
617 Proteinase K (1 µg/ml), respectively, post-fixed for 20 minutes in BT fix, and incubated in
618 acetone/ethanol mix (1:2) for 15 minutes at -20°C. The samples were equilibrated for 1 hour at
619 room temperature in equilibration buffer, incubated for 90 minutes at 37°C in reaction solution
620 (16 µl TdT enzyme + 38 µl reaction buffer). The reaction was stopped by addition of 200 µl stop

621 buffer overnight at 37°C. The samples were blocked for 2 hours and incubated overnight at 4°C
622 with an anti-DIG coupled to HRP. After several washes in PBST, the reaction product was
623 detected with DAB as a substrate.

624 **EDU labeling**

625 EdU was added at 50 hpf directly to the Embryo Medium at a final concentration of 0.1 mg/ml.
626 Experimental samples were incubated during 1 hour at 20°C and then rinsed 3 times in Embryo
627 Medium. After incubation, samples were split evenly into two experimental groups, pulse and
628 chase, respectively, and raised at 28.5ºC. Pulse group samples were then fixed at 52 hpf.
629 Chase group samples were fixed at 72 hpf. The Click-iT EdU Imaging Kit (Thermo Fisher
630 Scientific, Waltham, MA) was used to process the EdU label in whole fixed zebrafish prior to
631 antibody staining, according to the manufacturer's protocols.
632

633 **Spinning disk imaging**

634 A Leica SD6000 spinning disk confocal with Borealis illumination technology was used to image
635 live embryos and larvae. Fish from a single clutch were used for imaging only at one stage to
636 prevent stress-induced developmental delay. Larvae were anesthetized in 80 mg/l clove oil
637 (Hilltech), mounted in 0.7% agarose in glass-bottomed Petri dishes, covered with E2 containing
638 clove oil, and, for time-lapse microscopy, imaged at 20-minute intervals. Larvae imaged in this
639 manner appeared similar to staged, non-imaged controls. Videos were constructed from z-
640 projections using Metamorph imaging software (Molecular Devices).
641

642 **Metabolomics**

643 *Sample processing.* Prior to extraction, 450 individual zebrafish larvae were pooled to provide
644 enough material for metabolomics analysis (n=5 for wild type and mutant). Larvae were
645 transferred to 2.0 mL Sorenson low-binding microcentrifuge tubes. Cellular homogenization

646 was conducted by adding 0.1 µl of 0.1 mm Zirconica/silica beads to each tube then processing
647 with a Bullet Blender (BB50-DX) at speed 10 for 3 minutes as suggested by Next Advance
648 protocols. The homogenization step was repeated. After the bead beating, the tubes were
649 visually inspected for complete homogenization. Metabolites and lipids were extracted using a
650 modified Folch extraction (MPLEx) [67,68]. The extracted polar metabolite layer was, dried *in*
651 *vacuo*, and stored at -20˚C until Mass Spectroscopy (MS) sample preparation. The total lipid
652 extract was reconstituted in 500 µl of 2:1 chloroform/methanol and stored at -20˚C until LC-MS
653 analysis.
654
655 *LC-MS/MS lipidomics analysis.* Prior to LC-MS analysis, lipid extracts were dried and then
656 reconstituted in 10 µl chloroform and 490 µl of methanol. LC-MS/MS parameters and lipid
657 identifications are outlined in [69]. To facilitate quantification of lipids, a list of lipids identified
658 from the MS/MS data was created, including lipid name, observed *m/z*, and retention time. Lipid
659 features from each analysis were then aligned based on their *m/z* and retention time using
660 MZmine 2 [70]. Aligned features were manually verified and peak apex intensity values were
661 exported for subsequent statistical analysis.
662
663 *GC-MS metabolomics analysis.* Dried metabolite extracts were chemically derivatized using a
664 modified protocol used to create the FiehnLib [71] as described [72]. Metabolite identifications
665 were manually validated with peak intensity values used for statistical analysis.
666
667 *Statistical analysis.* Metabolomics and lipidomics were analyzed separately and data were log2
668 transformed prior to further processing. Negative and positive mode lipidomics data were
669 processed separately. To identify any potential outlying samples, a robust Mahalanobis distance
670 (rMd) filter was applied [73] and analyzed on the basis of correlation, median absolute deviation,
671 and skew. One biological outlier was identified (WT replicate 4) in the metabolomics data and

confirmed via Pearson correlation between the samples, and was therefore removed from further processing. All data were normalized using global median centering. Metabolites and lipids were evaluated with Analysis of Variance (ANOVA) with a Holm p-value test correction [74].

ACKNOWLEDGEMENTS. This study was supported by NIH GM114438, NS093793, and TR001395; Intramural Research Program of the National Human Genome Research Institute; the Common Fund of the NIH Office of the Director. Lipidomics analyses were performed in the Environmental Molecular Sciences Laboratory, a national scientific user facility sponsored by the Department of Energy (DOE) Office of Biological and Environmental Research and located at Pacific Northwest National Laboratory (PNNL). PNNL is operated by Battelle Memorial Institute for the DOE under contract DEAC05-76RLO1830. We would like to thank Bruce Appel and Judith Eisen for sharing reagents and invaluable advice.

Author contributions:

B.B.-S. and M.W. conceptualized the project and B.B.-S. designed the experiments. B.B.-S., A.C., J.L.P., M.M. performed zebrafish immunohistochemistry, image analysis and quantification, and statistical analysis. S.J.S. performed behavior experiments with support from P.W. J.B.P., J.W. generated initial F0 generation. B.B.-S., A.C., J.L.P., M.M. established F1 mutant lines and maintained subsequent generations. E.M., Y.H., D.R.A., C.T., W.A.G, M.C.V.M, C.J.T. performed patient´s clinical evaluations. J.K., E.M.Z, K.J.B, K.G.S., D.K., T.O.M. performed lipidomics analysis. B.B.-S, M.W. wrote the manuscript. All authors reviewed and edited the manuscript.

695 **REFERENCES**

696 1. Zalc B (2016) The acquisition of myelin: An evolutionary perspective. Brain Res 1641: 4-10.

697 2. Hodgkin AL (1937) Evidence for electrical transmission in nerve: Part I. J Physiol 90: 183-
698 210.

699 3. Lillie RS (1925) Factors Affecting Transmission and Recovery in the Passive Iron Nerve
700 Model. J Gen Physiol 7: 473-507.

701 4. Seidl AH (2014) Regulation of conduction time along axons. Neuroscience 276: 126-134.

702 5. Zhou Q, Anderson DJ (2002) The bHLH transcription factors OLIG2 and OLIG1 couple
703 neuronal and glial subtype specification. Cell 109: 61-73.

704 6. Briscoe J, Pierani A, Jessell TM, Ericson J (2000) A homeodomain protein code specifies
705 progenitor cell identity and neuronal fate in the ventral neural tube. Cell 101: 435-445.

706 7. Park HC, Appel B (2003) Delta-Notch signaling regulates oligodendrocyte specification.
707 Development 130: 3747-3755.

708 8. Kucenas S, Snell H, Appel B (2008) nkx2.2a promotes specification and differentiation of a
709 myelinating subset of oligodendrocyte lineage cells in zebrafish. Neuron Glia Biol 4: 71-
710 81.

711 9. Lu QR, Sun T, Zhu Z, Ma N, Garcia M, et al. (2002) Common developmental requirement for
712 Olig function indicates a motor neuron/oligodendrocyte connection. Cell 109: 75-86.

713 10. Ravanelli AM, Appel B (2015) Motor neurons and oligodendrocytes arise from distinct cell
714 lineages by progenitor recruitment. Genes Dev 29: 2504-2515.

715 11. Touahri Y, Escalas N, Benazeraf B, Cochard P, Danesin C, et al. (2012) Sulfatase 1
716 promotes the motor neuron-to-oligodendrocyte fate switch by activating Shh signaling in
717 Olig2 progenitors of the embryonic ventral spinal cord. J Neurosci 32: 18018-18034.

718 12. Takebayashi H, Nabeshima Y, Yoshida S, Chisaka O, Ikenaka K, et al. (2002) The basic
719 helix-loop-helix factor olig2 is essential for the development of motoneuron and
720 oligodendrocyte lineages. Curr Biol 12: 1157-1163.

721 13. Hornig J, Frob F, Vogl MR, Hermans-Borgmeyer I, Tamm ER, et al. (2013) The transcription
722 factors Sox10 and Myrf define an essential regulatory network module in differentiating
723 oligodendrocytes. PLoS Genet 9: e1003907.
724 14. Weider M, Starost LJ, Groll K, Kuspert M, Sock E, et al. (2018) Nfat/calcineurin signaling
725 promotes oligodendrocyte differentiation and myelination by transcription factor network
726 tuning. Nat Commun 9: 899.
727 15. Liu Z, Hu X, Cai J, Liu B, Peng X, et al. (2007) Induction of oligodendrocyte differentiation by
728 Olig2 and Sox10: evidence for reciprocal interactions and dosage-dependent
729 mechanisms. Dev Biol 302: 683-693.
730 16. Tsai HH, Niu J, Munji R, Davalos D, Chang J, et al. (2016) Oligodendrocyte precursors
731 migrate along vasculature in the developing nervous system. Science 351: 379-384.
732 17. Kirby BB, Takada N, Latimer AJ, Shin J, Carney TJ, et al. (2006) In vivo time-lapse imaging
733 shows dynamic oligodendrocyte progenitor behavior during zebrafish development. Nat
734 Neurosci 9: 1506-1511.
735 18. Topilko P, Schneider-Maunoury S, Levi G, Baron-Van Evercooren A, Chennoufi AB, et al.
736 (1994) Krox-20 controls myelination in the peripheral nervous system. Nature 371: 796-
737 799.
738 19. Monk KR, Naylor SG, Glenn TD, Mercurio S, Perlin JR, et al. (2009) A G protein-coupled
739 receptor is essential for Schwann cells to initiate myelination. Science 325: 1402-1405.
740 20. Finzsch M, Schreiner S, Kichko T, Reeh P, Tamm ER, et al. (2010) Sox10 is required for
741 Schwann cell identity and progression beyond the immature Schwann cell stage. J Cell
742 Biol 189: 701-712.
743 21. Grove M, Kim H, Santerre M, Krupka AJ, Han SB, et al. (2017) YAP/TAZ initiate and
744 maintain Schwann cell myelination. Elife 6.
745 22. Jessen KR, Mirsky R (2005) The origin and development of glial cells in peripheral nerves.
746 Nat Rev Neurosci 6: 671-682.

747 23. Kao SC, Wu H, Xie J, Chang CP, Ranish JA, et al. (2009) Calcineurin/NFAT signaling is
748 required for neuregulin-regulated Schwann cell differentiation. Science 323: 651-654.
749 24. Salzer JL (2015) Schwann cell myelination. Cold Spring Harb Perspect Biol 7: a020529.
750 25. Parmantier E, Lynn B, Lawson D, Turmaine M, Namini SS, et al. (1999) Schwann cell-
751 derived Desert hedgehog controls the development of peripheral nerve sheaths. Neuron
752 23: 713-724.
753 26. Kucenas S, Takada N, Park HC, Woodruff E, Broadie K, et al. (2008) CNS-derived glia
754 ensheath peripheral nerves and mediate motor root development. Nat Neurosci 11: 143-
755 151.
756 27. Shanthaveerappa TR, Bourne GH (1962) A perineural epithelium. J Cell Biol 14: 343-346.
757 28. Burkel WE (1967) The histological fine structure of perineurium. Anat Rec 158: 177-189.
758 29. Kucenas S (2015) Perineurial glia. Cold Spring Harb Perspect Biol 7.
759 30. Clark JK, O'Keefe A, Mastracci TL, Sussel L, Matise MP, et al. (2014) Mammalian Nkx2.2+
760 perineurial glia are essential for motor nerve development. Dev Dyn 243: 1116-1129.
761 31. Baker SJ (2003) Small unstable apoptotic protein, an apoptosis-associated protein,
762 suppresses proliferation of myeloid cells. Cancer Res 63: 705-712.
763 32. Hosono K, Sasaki T, Minoshima S, Shimizu N (2004) Identification and characterization of a
764 novel gene family YPEL in a wide spectrum of eukaryotic species. Gene 340: 31-43.
765 33. Kelley KD, Miller KR, Todd A, Kelley AR, Tuttle R, et al. (2010) YPEL3, a p53-regulated
766 gene that induces cellular senescence. Cancer Res 70: 3566-3575.
767 34. Tuttle R, Miller KR, Maiorano JN, Termuhlen PM, Gao Y, et al. (2012) Novel senescence
768 associated gene, YPEL3, is repressed by estrogen in ER+ mammary tumor cells and
769 required for tamoxifen-induced cellular senescence. Int J Cancer 130: 2291-2299.
770 35. Zhang J, Wen X, Ren XY, Li YQ, Tang XR, et al. (2016) YPEL3 suppresses epithelial-
771 mesenchymal transition and metastasis of nasopharyngeal carcinoma cells through the
772 Wnt/beta-catenin signaling pathway. J Exp Clin Cancer Res 35: 109.

773 36. Rowitch DH, Kriegstein AR (2010) Developmental genetics of vertebrate glial-cell
774 specification. Nature 468: 214-222.
775 37. Jessell TM (2000) Neuronal specification in the spinal cord: inductive signals and
776 transcriptional codes. Nat Rev Genet 1: 20-29.
777 38. Danesin C, Soula C (2017) Moving the Shh Source over Time: What Impact on Neural Cell
778 Diversification in the Developing Spinal Cord? J Dev Biol 5.
779 39. Stednitz SJ, McDermott EM, Ncube D, Tallafuss A, Eisen JS, et al. (2018) Forebrain Control
780 of Behaviorally Driven Social Orienting in Zebrafish. Curr Biol 28: 2445-2451 e2443.
781 40. Zannino DA, Appel B (2009) Olig2+ precursors produce abducens motor neurons and
782 oligodendrocytes in the zebrafish hindbrain. J Neurosci 29: 2322-2333.
783 41. Flanagan-Steet H, Fox MA, Meyer D, Sanes JR (2005) Neuromuscular synapses can form
784 in vivo by incorporation of initially aneural postsynaptic specializations. Development
785 132: 4471-4481.
786 42. Qi Y, Cai J, Wu Y, Wu R, Lee J, et al. (2001) Control of oligodendrocyte differentiation by
787 the Nkx2.2 homeodomain transcription factor. Development 128: 2723-2733.
788 43. Lyons DA, Naylor SG, Scholze A, Talbot WS (2009) Kif1b is essential for mRNA localization
789 in oligodendrocytes and development of myelinated axons. Nat Genet 41: 854-858.
790 44. Ackerman SD, Garcia C, Piao X, Gutmann DH, Monk KR (2015) The adhesion GPCR
791 Gpr56 regulates oligodendrocyte development via interactions with Galpha12/13 and
792 RhoA. Nat Commun 6: 6122.
793 45. Czopka T, Ffrench-Constant C, Lyons DA (2013) Individual oligodendrocytes have only a
794 few hours in which to generate new myelin sheaths in vivo. Dev Cell 25: 599-609.
795 46. Hughes EG, Kang SH, Fukaya M, Bergles DE (2013) Oligodendrocyte progenitors balance
796 growth with self-repulsion to achieve homeostasis in the adult brain. Nat Neurosci 16:
797 668-676.

798 47. Grosch S, Schiffmann S, Geisslinger G (2012) Chain length-specific properties of
799 ceramides. Prog Lipid Res 51: 50-62.
800 48. Ben-David O, Futerman AH (2010) The role of the ceramide acyl chain length in
801 neurodegeneration: involvement of ceramide synthases. Neuromolecular Med 12: 341-
802 350.
803 49. Bansal R, Winkler S, Bheddah S (1999) Negative regulation of oligodendrocyte
804 differentiation by galactosphingolipids. J Neurosci 19: 7913-7924.
805 50. Ravanelli AM, Kearns CA, Powers RK, Wang Y, Hines JH, et al. (2018) Sequential
806 specification of oligodendrocyte lineage cells by distinct levels of Hedgehog and Notch
807 signaling. Dev Biol 444: 93-106.
808 51. Chrast R, Saher G, Nave KA, Verheijen MH (2011) Lipid metabolism in myelinating glial
809 cells: lessons from human inherited disorders and mouse models. J Lipid Res 52: 419-
810 434.
811 52. Gahl WA, Tifft CJ (2011) The NIH Undiagnosed Diseases Program: lessons learned. Jama
812 305: 1904-1905.
813 53. Gahl WA, Markello TC, Toro C, Fajardo KF, Sincan M, et al. (2012) The National Institutes
814 of Health Undiagnosed Diseases Program: insights into rare diseases. Genet Med 14:
815 51-59.
816 54. Gahl WA, Mulvihill JJ, Toro C, Markello TC, Wise AL, et al. (2016) The NIH Undiagnosed
817 Diseases Program and Network: Applications to modern medicine. Mol Genet Metab
818 117: 393-400.
819 55. Pemberton PJV, E.; Bone, W. P.; Markello, C. J.; Flynn, E. D.; Links, A. E.; Boerkoel, C. F.;
820 Adams, D. R.; Gahl, W. A.; Markello, T. C., NIH Intramural Sequencing Center, NIH
821 Genomics Core, UDP Clinical Team (2014) Diploid alignment of whole human genome
822 data. 64th Annual Meeting of the American Society of Human Genetics. San Diego.

823 56. McKenna A, Hanna M, Banks E, Sivachenko A, Cibulskis K, et al. (2010) The Genome
824 Analysis Toolkit: a MapReduce framework for analyzing next-generation DNA
825 sequencing data. Genome Res 20: 1297-1303.
826 57. DePristo MA, Banks E, Poplin R, Garimella KV, Maguire JR, et al. (2011) A framework for
827 variation discovery and genotyping using next-generation DNA sequencing data. Nat
828 Genet 43: 491-498.
829 58. Van der Auwera GA, Carneiro MO, Hartl C, Poplin R, Del Angel G, et al. (2013) From FastQ
830 data to high confidence variant calls: the Genome Analysis Toolkit best practices
831 pipeline. Curr Protoc Bioinformatics 11: 11 10 11-11 10 33.
832 59. Cingolani P, Platts A, Wang le L, Coon M, Nguyen T, et al. (2012) A program for annotating
833 and predicting the effects of single nucleotide polymorphisms, SnpEff: SNPs in the
834 genome of Drosophila melanogaster strain w1118; iso-2; iso-3. Fly (Austin) 6: 80-92.
835 60. Richards S, Aziz N, Bale S, Bick D, Das S, et al. (2015) Standards and guidelines for the
836 interpretation of sequence variants: a joint consensus recommendation of the American
837 College of Medical Genetics and Genomics and the Association for Molecular Pathology.
838 Genet Med 17: 405-424.
839 61. Westerfield M (2007) The Zebrafish Book: A Guide for the Laboratory Use of Zebrafish
840 (Danio rerio), 5 edn (Eugene: University of Oregon Press).
841 62. Kimmel CB, Ballard WW, Kimmel SR, Ullmann B, Schilling TF (1995) Stages of embryonic
842 development of the zebrafish. Dev Dyn 203: 253-310.
843 63. Thisse C, Thisse B (2008) High-resolution in situ hybridization to whole-mount zebrafish
844 embryos. Nat Protoc 3: 59-69.
845 64. Strahle U, Blader P, Adam J, Ingham PW (1994) A simple and efficient procedure for non-
846 isotopic in situ hybridization to sectioned material. Trends Genet 10: 75-76.

847 65. Blanco-Sanchez B, Clement A, Fierro J, Jr., Washbourne P, Westerfield M (2014)
848 Complexes of Usher proteins preassemble at the endoplasmic reticulum and are
849 required for trafficking and ER homeostasis. Dis Model Mech 7: 547-559.
850 66. Cunliffe VT, Casaccia-Bonnefil P (2006) Histone deacetylase 1 is essential for
851 oligodendrocyte specification in the zebrafish CNS. Mech Dev 123: 24-30.
852 67. Folch J, Lees M, Sloane Stanley GH (1957) A simple method for the isolation and
853 purification of total lipides from animal tissues. J Biol Chem 226: 497-509.
854 68. Nakayasu ES, Nicora CD, Sims AC, Burnum-Johnson KE, Kim YM, et al. (2016) MPLEx: a
855 Robust and Universal Protocol for Single-Sample Integrative Proteomic, Metabolomic,
856 and Lipidomic Analyses. mSystems 1.
857 69. Kyle JE, Crowell KL, Casey CP, Fujimoto GM, Kim S, et al. (2017) LIQUID: an-open source
858 software for identifying lipids in LC-MS/MS-based lipidomics data. Bioinformatics 33:
859 1744-1746.
860 70. Pluskal T, Castillo S, Villar-Briones A, Oresic M (2010) MZmine 2: modular framework for
861 processing, visualizing, and analyzing mass spectrometry-based molecular profile data.
862 BMC Bioinformatics 11: 395.
863 71. Kind T, Wohlgemuth G, Lee DY, Lu Y, Palazoglu M, et al. (2009) FiehnLib: mass spectral
864 and retention index libraries for metabolomics based on quadrupole and time-of-flight
865 gas chromatography/mass spectrometry. Anal Chem 81: 10038-10048.
866 72. Webb-Robertson BJ, Kim YM, Zink EM, Hallaian KA, Zhang Q, et al. (2014) A Statistical
867 Analysis of the Effects of Urease Pre-treatment on the Measurement of the Urinary
868 Metabolome by Gas Chromatography-Mass Spectrometry. Metabolomics 10: 897-908.
869 73. Matzke MM, Waters KM, Metz TO, Jacobs JM, Sims AC, et al. (2011) Improved quality
870 control processing of peptide-centric LC-MS proteomics data. Bioinformatics 27: 2866-
871 2872.

74. HOLM S (1979) A Simple Sequentially Rejective Multiple Test Procedure. Scand J Statist 6: 65-70.

874 **FIGURES LEGENDS**

875

876 **Fig 1: YPEL3 is an evolutionary conserved disease-causing candidate gene. A:** MRI of
877 patient showing greatly enlarged brachial plexus. Arrows indicate the thick peripheral nerves. **B:**
878 Representative brain MRI (axial, T2-weighted) showing poor delineation of white and gray
879 matter, indicating delayed myelination. **C-E:** *ypel3* is maternally deposited and expressed during
880 neural development in zebrafish. **C:** Two-cell stage embryo. **D-E:** Transverse sections. **D:** At 24
881 hours postfertilization (hpf), *ypel3* expression is detected in the ventricular and mantle regions of
882 the developing spinal cord, and in cells where the motor roots develop (red arrow). **E:** At 56 hpf
883 (E), *ypel3* is expressed in the spinal cord and in the developing motor roots (red arrows). **F:**
884 Diagram of spinal cord domains, their derivatives, and molecular markers. The pMN domain
885 (*olig 2*+) gives rise first to motoneurons, and then later oligodendrocytes (Briscoe et al., 2000;
886 Jessell, 2000; Danesin and Soula, 2017). The p3 domain (*nkx2.2*+) is localized ventral to the
887 pMN domain and gives rise to oligodendrocytes and perineurial cells (Clark et al., 2014;
888 Kucenas et al., 2008b). **G:** Chromatogram of DNA from a heterozygous zebrafish carrier
889 showing INDEL created using CRISPR/Cas9 technology. **H:** Protein alignment of human long
890 isoform (Hsa-2) and zebrafish (Dre) and human (Hsa-1) short isoforms. Arrow shows the
891 location of the p.Val92Serfs*38 mutation in the YPEL3 long isoform. Inset shows the amino
892 acids encoded by the *ypel3*^{b1310} allele that causes the p.Gly95Argfs*4 mutation in the long
893 zebrafish isoform. Scale bar: 250µm in C, 25µm in D, E.

894

895 **Fig 2: Adult maternal-zygotic *ypel3*$^{-/-}$ mutants have behavioral and locomotion defects.**
896 **A-C:** Representative swimming traces of wild type (WT, A), heterozygous *ypel3*^{b1309} (B), and
897 homozygous maternal-zygotic *ypel3*^{b1309} mutants (C). **D-F:** Quantification of total distance
898 traveled (D), average relative distance from the surface (E), and percent time spent in motion

899 (F). +/+: WT. +/-: heterozygous. -/-: maternal-zygotic *ypel3* mutants. Bars represent +/-
900 standard error of the mean (+/- SEM).
901
902 **Fig 3: Specification and differentiation of motoneurons are unaffected in maternal-**
903 **zygotic *ypel3* mutants. A-F:** Analysis of the pMN domain and its derivatives. Transverse
904 sections. **A-C:** WT. **D-F:** maternal zygotic (mz) *ypel3*$^{-/-}$. **A, D:** pMN domain and its derivatives
905 labeled by *olig2:kaede* transgene. **B, E:** Topro nuclear labeling. **C, F:** Merge. **G-J:** Analysis of
906 motoneuron differentiation in mz *ypel3* mutants. Lateral views. Motoneurons are labeled by the
907 *mnx1:gfp* transgene. **G, H:** WT embryo at 26 hpf (G) and larva at 52 hpf (H). **I, J**: mz *ypel3*
908 mutant at 26 hpf (I) and larva at 52 hpf (J). Images were taken at the level of somites 6 to10. **K-**
909 **L:** Quantification of the number of motoneurons at 26 hpf (K) and at 52 hpf (L). Bars show +/-
910 SEM. Scale bars: 5µm in A, B, D and E. 25µm in G-J.
911
912 **Fig 4: *ypel3* is required for myelinating oligodendrocyte specification. A, B:** WT larvae at
913 52 hpf (A) and at 72 hpf (B). **C, D:** mz *ypel3* mutants at 52 hpf (C) and at 72 hpf (D).
914 Arrowheads show myelinating oligodendrocyte progenitor cells (OPCs; double mRFP, mGFP
915 positive cells) in A, C. Black arrows show myelinating oligodendrocytes expressing *mbpb* in B,D.
916 Scale bars: 25µm. Images are lateral views. **E-H:** Quantification of the number of OPCs at 52
917 hpf (E), *mbpb* expressing cells at 72 hpf (F), Edu positive cells at 52 hpf (G) and 72 hpf (H).
918 Bars represent +/- SEM.
919
920 **Fig 5: Ypel3 is required for proper maturation of Schwann cell precursors.**
921 **A, B:** *sox10* mRNA *in situ* hybridization in WT (A) and mz *ypel3* mutant (B) showing maintained
922 *sox10* expression (arrows) in the mz *ypel3* mutant at 26 hpf. **C, D:** Schwann cell precursors
923 migrate correctly in the region of the developing motor roots in the mz *ypel3* mutant. WT (C) and
924 mz *ypel3* mutant (D) embryos at 26 hpf**.** Arrows indicate Schwann cell precursors. **E, F:** Initial

925 ensheathing of motor axons by Schwann cells occurs properly in the mz *ypel3* mutant. WT (E)
926 and mz *ypel3* mutant (F) larvae at 56 hpf**.** Arrows indicate Schwann cells ensheathing motor
927 axons. Arrowhead: blood vessel. **G, H:** Schwann cells fail to form normal structures in the mz
928 *ypel3* mutant. At 5dpf, in WT (G), Schwann cells form slender rod-like structures (arrows). At
929 this stage, the mRFP signal has cleared from the ventral myotome. In the mz *ypel3* mutant (F),
930 Schwann cells fail to wrap the motor axon tightly and *sox10* expression as indicated by mRFP is
931 maintained within the ventral region of the myotome. Yellow horizontal line: spinal cord ventral
932 border. White horizontal dashed line: horizontal myoseptum. Yellow dashed lines outline
933 melanocytes. All images are lateral views. Scale bars: 25 µm. **I:** Quantification of the average
934 number of motor nerves per somite labeled with *sox10:mRFP* at 56 hpf. **J:** Quantification of the
935 average number of motor nerves per somite labeled with *sox10:mRFP* at the level of ventral
936 myotome. Bars represent +/-SEM.
937
938 **Fig 6: Ypel3 is required for perineurial glia ensheathing. A:** WT larva at 56 hpf. Perineurial
939 glia (expressing *nkx2.2a:GFP*, green) have migrated out of the CNS and begun to ensheath the
940 motor nerve. White arrow points to perineurial glia associated with the immature motor nerve. **B:**
941 mz *ypel3*$^{-/-}$ mutant at 56 hpf. At this stage, perineurial glia are largely absent, and the few that
942 migrate out of the CNS appear wispy and thin (yellow arrow). **C:** In WT larvae at 5dpf,
943 perineurial glia are tightly associated with Schwann cells (expressing *sox10:mRFP*, red) forming
944 slender tubes (white arrow). **D:** In mz *ypel3*$^{-/-}$ mutant, at 5dpf, perineurial glia are overgrown and
945 fail to associate with the Schwann cells. White horizontal dashed line: horizontal myoseptum.
946 Yellow dashed lines label the somite boundaries. Scale bar: 25 µm **E-F:** Quantification of the
947 average number of motor nerves per somite labeled with GFP (E) and the average number of
948 motor nerves per somite with slender tube morphology (F). **G-G'':** WT larvae at 7dpf. Perineurial
949 glia have completely wrapped the Schwann cells forming a tubular structure (arrow). Some
950 mRFP expression remains within the mature Schwann cells. **G:** Merge. **G':** mRFP expression is

951 clustered within the GFP positive domain (outlined with white dashed lines), which is composed
952 of perineurial cells. **G'':** Perineurial cells form a tubular structure (outlined with white dashed
953 lines). **H-H'':** mz *ypel3* mutant at 7dpf. Perineurial glia are overgrown and form a defasciculated
954 structure. **H:** Merge. **H':** mRFP signal is elevated in the mz *ypel3* mutant Schwann cells and
955 delineates three defasciculated structures (1, 2, 3). **H'':** mz *ypel3* mutant perineurial glia fail to
956 wrap Schwann cells correctly resulting in an enlarged nerve (outlined with white dashed lines).
957 White horizontal line in A-D, G-G'': spinal cord ventral border. White horizontal dashed line in A-
958 D: horizontal myoseptum. SC: spinal cord. *: loose perineurial cells. All images are lateral views.
959 Scale bars: 25 µm in A-D, 5µm in G-H''.
960
961 **Fig 7: Ypel3 is required for central and peripheral myelination. A-D:** Myelin basic protein b
962 (Mbpb) expression. Lateral views of embryos labeled for Mbpb at 7 dpf. **A:** WT. **B-D:** mz *ypel3*
963 mutants. Mbpb levels are reduced in the spinal cord (sc) and variably reduced in the motor
964 nerves (arrows). Yellow arrow shows a fasciculated nerve with a homogenous distribution of the
965 Mbpb signal. White arrows show defasciculated nerves in mz *ypel3* mutants. Mutant nerves
966 have variable levels and an uneven distribution of Mbpb. White horizontal dashed line in A-D:
967 spinal cord ventral border. Yellow dashed chevron: somite boundary. Scale bar: 25µm. **E:**
968 Lipidomics panel showing an increase in phosphatic acids (PA) and ceramides (Cer) in the mz
969 *ypel3* mutant compared to WT.
970
971 **Supplementary Fig 1**: ***ypel3^{b1309}* and *ypel3^{b1310}* CRISPR engineered alleles are equivalent**
972 **to the *YPEL3* variant. A) Alignment of human and zebrafish YPEL3 protein variants.** The
973 *YPEL3* gene encodes two transcript variants: a long variant (NM_031477) that gives rise to a
974 protein composed of 157 amino acids (NP_113665.3) and a short variant (NM_001145524) that
975 encodes a protein of 119 amino acids (NP_001138996.10. One zebrafish *ypel3* transcript
976 variant (NM_212790.1) has been characterized to date. It encodes a protein of 119 amino acids

977 (NP_997955.1). TV1: Long human YPEL3 protein variant. TV2: Short human YPEL3 protein
978 variant. danio: Ypel3 zebrafish protein. Blue arrowhead indicates the human variant that results
979 in p.V92Sfs*38 based on the long human protein isoform. **B) Zebrafish mutant alleles created**
980 **by CRISPR/Cas9 technology.** Two alleles were generated using the same single guide RNA.
981 Both *ypel3*^{b1309} and *ypel3*^{b1310} are frameshift mutations, p.N56Ffs*1 and p.G60Rfs*4,
982 respectively.
983

984 **Supplementary figure 2: The width of motor axon fascicles is not affected in the**
985 **mz *ypel3* mutants.** A, B: Quantification of motor axon width or thickness in WT and mz ypel3
986 mutants at 26 (A) and 52 (B) hpf.

987

988 **Supplementary videos 1 and 2: Ypel3 is required for OPC and perineurial glia**
989 **development.** Supplementary video 1: WT. Supplementary video 2: mz *ypel3* mutant. Time-
990 lapse videos from 50 to 62 hpf. Each frame is a projection of a 50 µm deep Z-stack of lateral
991 views acquired every 25 minutes using a spinning disk microscope. Dark yellow arrows indicate
992 OPCs. Green arrows indicate perineurial glial cells that have exited the CNS. Scale bar: 20µm.

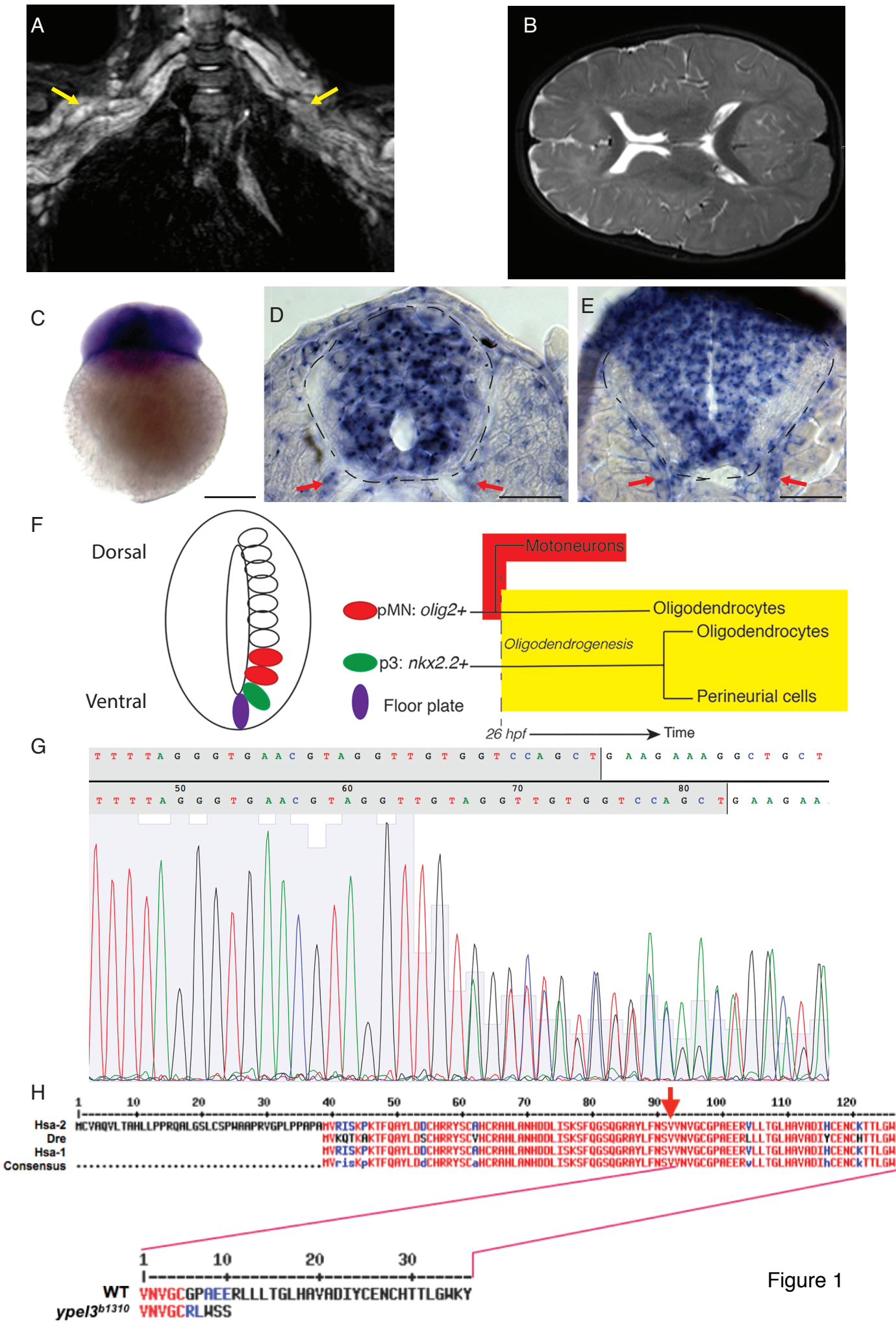
A
B
C
D
E
F
Dorsal
Ventral
pMN: olig2+
p3: nkx2.2+
Floor plate
Motoneurons
Oligodendrocytes
Oligodendrocytes
Oligodendrogenesis
Perineurial cells
26 hpf
Time
G
H
Hsa-2
Dre
Hsa-1
Consensus
WT
ypel3b1310
YNVGCGPAEERLLLTGLHAVADIYCENCHTTLGWKY
YNVGCRLWSS

Figure 1

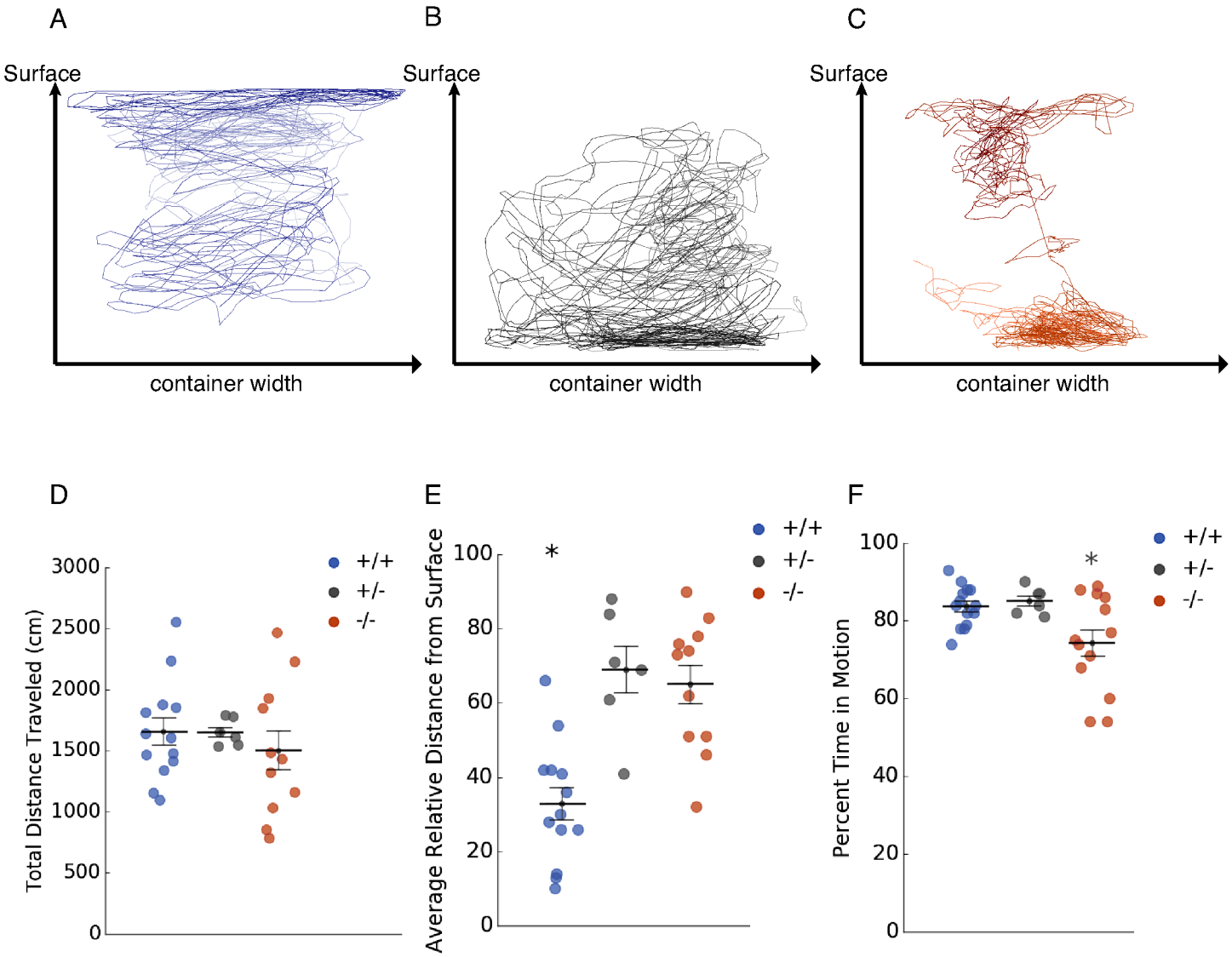
A
Surface
container width
B
Surface
container width
C
Surface
container width
D
Total Distance Traveled (cm)
3000
2500
2000
1500
1000
500
0
+/+
+/-
-/-
E
Average Relative Distance from Surface
100
80
60
40
20
0
*
+/+
+/-
-/-
F
Percent Time in Motion
100
80
60
40
20
0
*
+/+
+/-
-/-

Figure 2

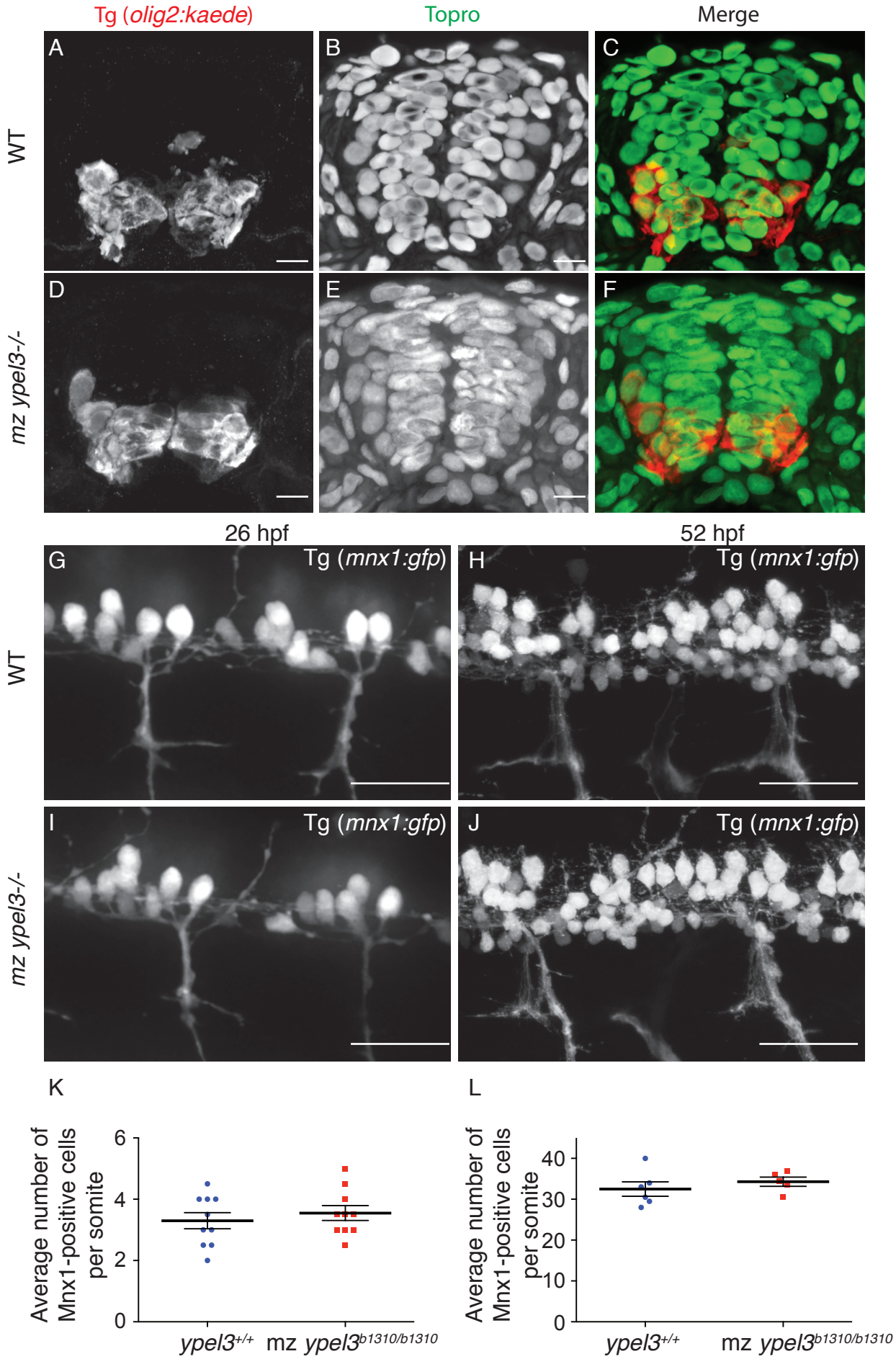
Tg (olig2:kaede)
Topro
Merge
A
B
C
D
E
F
WT
mz ypel3-/-
26 hpf
52 hpf
G
H
I
J
Tg (mnx1:gfp)
K
L
Average number of Mnx1-positive cells per somite
0
2
4
6
10
20
30
40
ypel3+/+
mz ypel3b1310/b1310

Figure 3

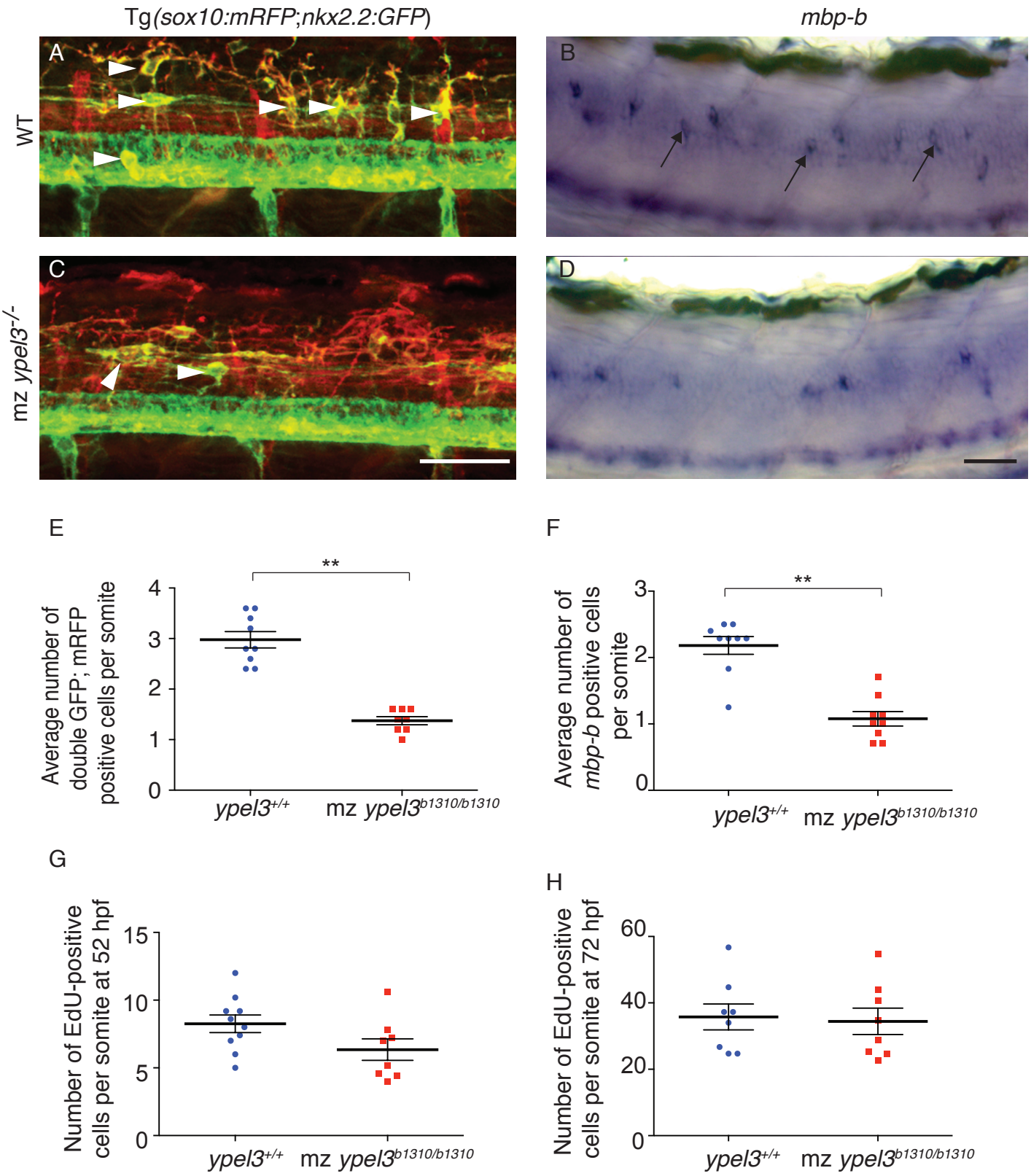
Tg(sox10:mRFP;nkx2.2:GFP)
mbp-b
A
B
C
D
WT
mz ypel3-/-
E
F
G
H
Average number of double GFP; mRFP positive cells per somite
Average number of mbp-b positive cells per somite
Number of EdU-positive cells per somite at 52 hpf
Number of EdU-positive cells per somite at 72 hpf
**
ypel3+/+
mz ypel3b1310/b1310

Figure 4

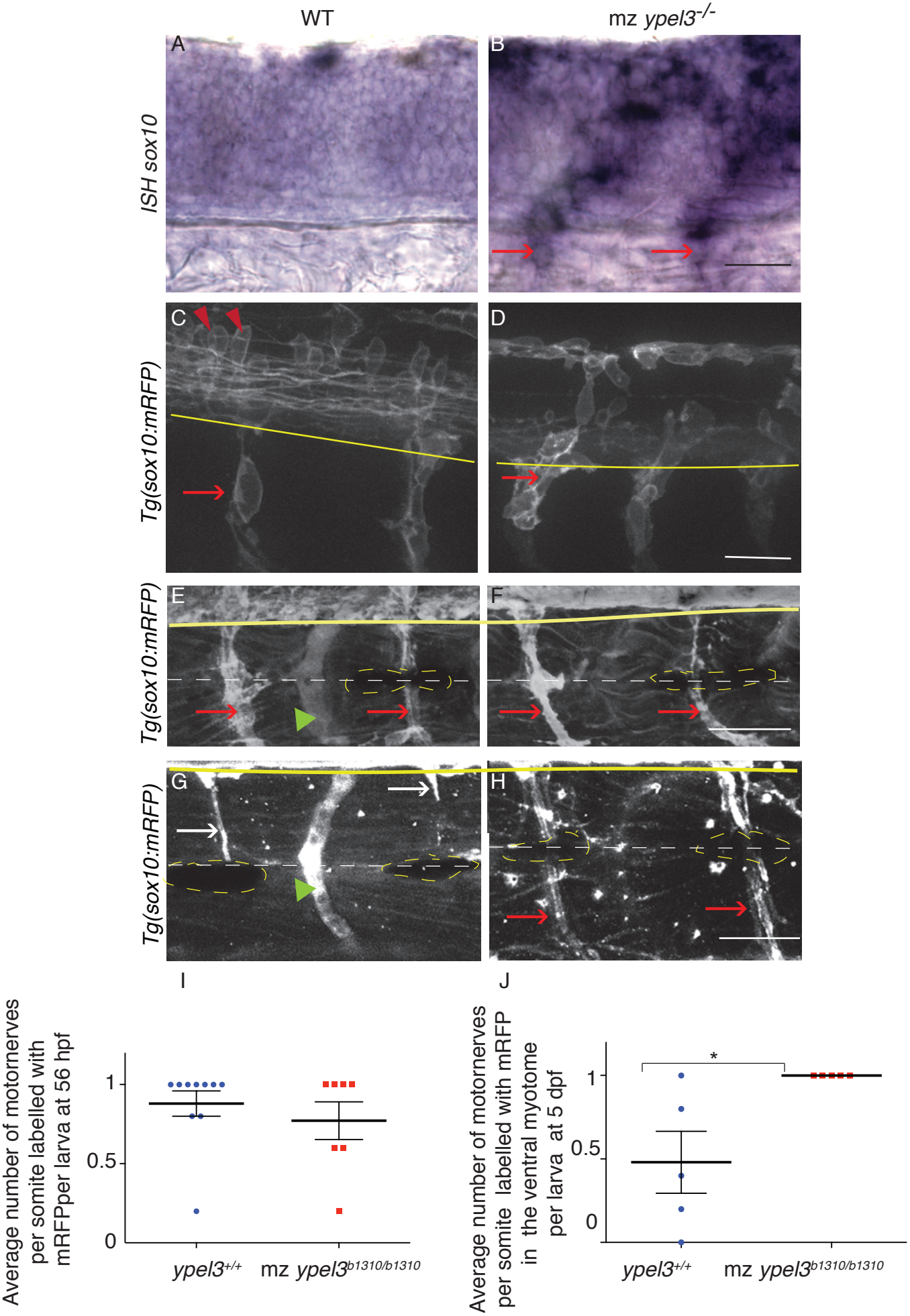
WT
mz ypel3-/-
A
B
ISH sox10
C
D
Tg(sox10:mRFP)
E
F
Tg(sox10:mRFP)
G
H
Tg(sox10:mRFP)
I
Average number of motornerves per somite labelled with mRFPper larva at 56 hpf
1
0.5
0
ypel3+/+
mz ypel3b1310/b1310
J
Average number of motornerves per somite labelled with mRFP in the ventral myotome per larva at 5 dpf
*
1
0.5
0
ypel3+/+
mz ypel3b1310/b1310

Figure 5

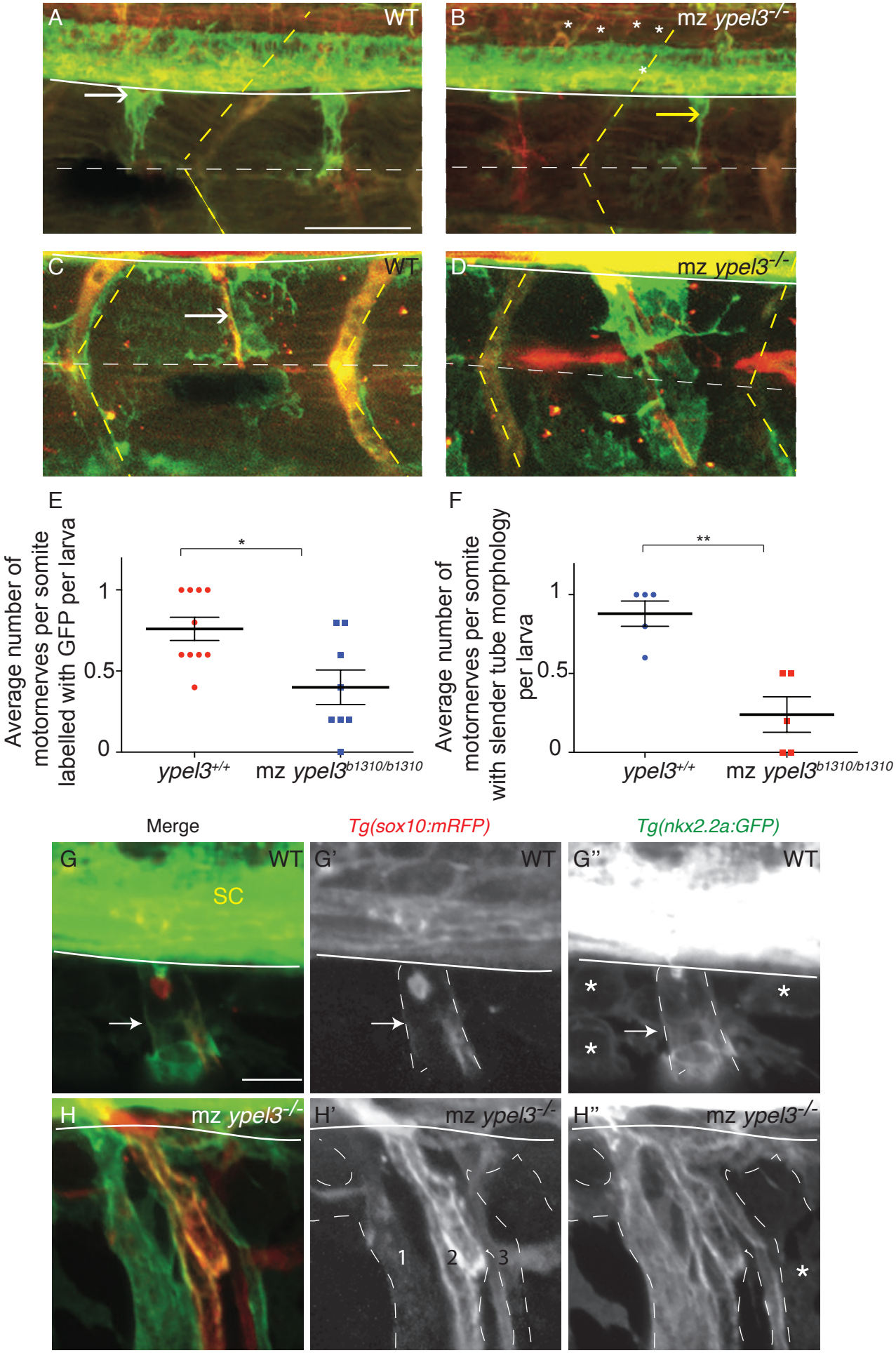
A
WT
B
mz ypel3-/-
C
WT
D
mz ypel3-/-
E
Average number of motornerves per somite labelled with GFP per larva
1
0.5
0
*
ypel3+/+
mz ypel3b1310/b1310
F
Average number of motornerves per somite with slender tube morphology per larva
1
0.5
0
**
ypel3+/+
mz ypel3b1310/b1310
Merge
Tg(sox10:mRFP)
Tg(nkx2.2a:GFP)
G
WT
SC
G'
WT
G''
WT
H
mz ypel3-/-
H'
mz ypel3-/-
1
2
3
H''
mz ypel3-/-

Figure 6

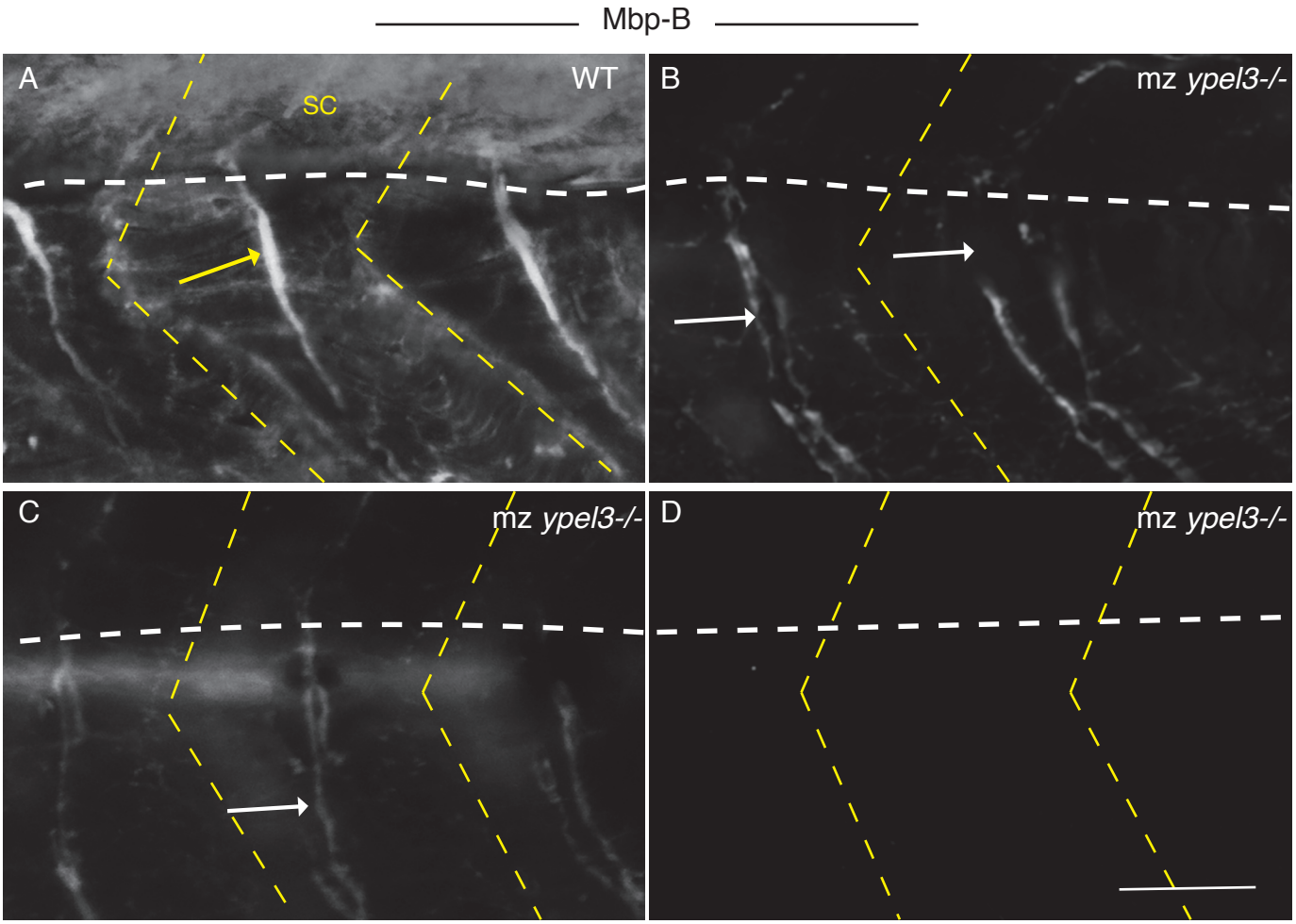

E

LipidName	Fold_change
PA(20:5/22:6)	0.57
PA(16:0/22:6)	0.51
PA(22:6/22:6)	0.46
Cer(d18:1/26:0)	0.34
Cer(d18:1/25:0)	0.22
Cer(d18:1/20:0)	-0.14
SM(d18:1/26:0)	0.36
SM(d18:1/25:0)	0.19
SM(d18:1/26:1)	0.09

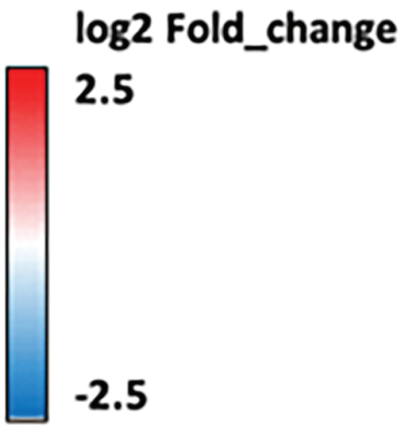

Figure 7

A

```
           1        10        20        30        40        50        60        70        80        90       100       110       120       130
           |--------+---------+---------+---------+---------+---------+---------+---------+---------+---------+---------+---------+---------|
     TV1   MCVAQVLTAHLLPPRQALGSLCSPWAAPRVGPLPPAPAMVRISKPKTFQAYLDDCHRRYSCAHCRAHLANHDDLISKSFQGSQGRAYLFNSVVNVGCGPAEERVLLTGLHAVADIHCENCKTTLGWKYEQ
    danio                                        MVKQTKAKTFQAYLDSCHRRYSCVHCRAHLANHDDLISKSFQGSQGRAYLFNSVVNVGCGPAEERLLLTGLHAVADIYCENCHTTLGWKYEQ
     TV2                                         MVRISKPKTFQAYLDDCHRRYSCAHCRAHLANHDDLISKSFQGSQGRAYLFNSVVNVGCGPAEERVLLTGLHAVADIHCENCKTTLGWKYEQ
Consensus  ......................................MVrisKpKTFQAYLDdCHRRYSCaHCRAHLANHDDLISKSFQGSQGRAYLFNSVVNVGCGPAEERvLLTGLHAVADIhCENCkTTLGWKYEQ

           131     140       150     157
           |--------+---------+------|
     TV1   AFESSQKYKEGKYIIELNHMIKDNGWD
    danio  AFELSQKYKEGKFIIELSHMIKDNGWD
     TV2   AFESSQKYKEGKYIIELNHMIKDNGWD
Consensus  AFEsSQKYKEGK%IIELnHMIKDNGWD
```

B

```
           261     270       280       290       300       310       320       330       340       350       360       370       380       390
           |--------+---------+---------+---------+---------+---------+---------+---------+---------+---------+---------+---------+---------|
        wt ATTTTGTGTTTTTAGGGTGAACG-TAGGTTGT-------GGTCCAGCTGAAGAAAGGCTGCTGCTTACTGGTCTTCATGCTGTGGCTGATATTTATTGTGAGAATTACTGGGCTGGAAATACGTGAGTAT
    b1309 ATTTTGTGTTTTTAGGTAGGTTGGTAGGTTGT-------GGTCCAGCTGAAGAAAGGCTGCTGCTTACTGGTCTTCATGCTGTGGCTGATATTTATTGTGAGAATTACTGGGCTGGAAATACGTGAGTAT
    b1310 ATTTTGTGTTTTTAGGGTGAACG-TAGGTTGTAGGTTGTGGTCCAGCTGAAGAAAGGCTGCTGCTTACTGGTCTTCATGCTGTGGCTGATATTTATTGTGAGAATTACTGGGCTGGAAATACGTGAGTAT
Consensus ATTTTGTGTTTTTAGGgtGaacG.TAGGTTGT.......GGTCCAGCTGAAGAAAGGCTGCTGCTTACTGGTCTTCATGCTGTGGCTGATATTTATTGTGAGAATTACTGGGCTGGAAATACGTGAGTAT
```

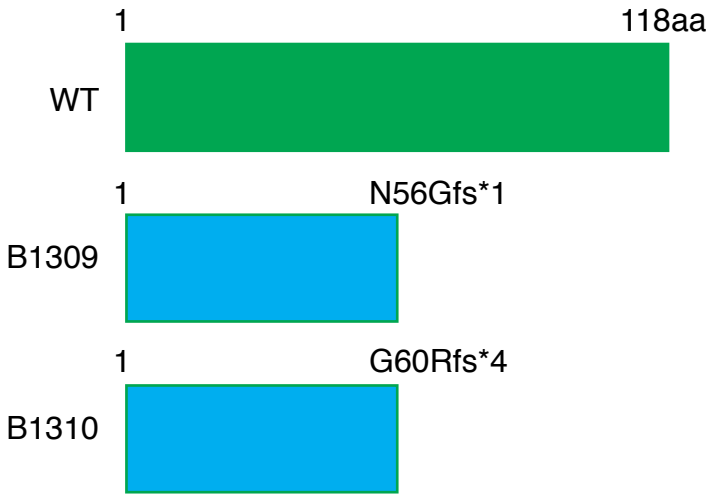

Supplementary figure 1

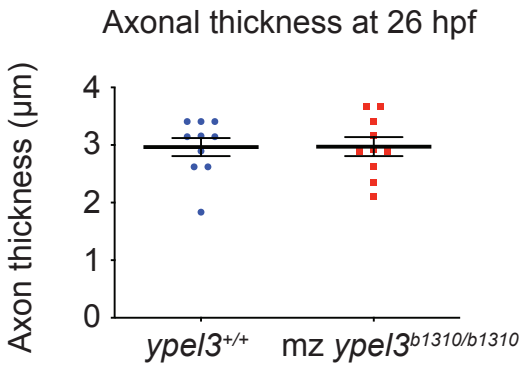

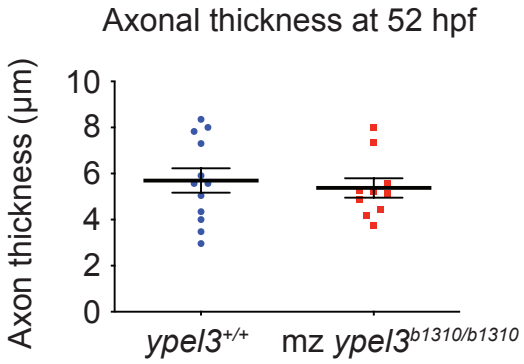

Supplementary figure 2

Supplementary Video 1

Click here to access/download
Other
Sup video 1.avi

Supplementary Video 2

Click here to access/download

Other

Sup video 2.avi